Gondwana Research 27 (2015) 258–280

Contents lists available at ScienceDirect

Gondwana Research

journal homepage: www.elsevier.com/locate/gr

Multi-pulse cotectic evolution and in-situ fractionation of calc-alkaline tonalite–granodiorite rocks, Sierra de Velasco batholith, Famatinian belt, Argentina

Laura Iudith Bellos [a,*], Antonio Castro [b], Juan Díaz-Alvarado [c], Alejandro Toselli [a]

[a] INSUGEO-CONICET, Facultad de Ciencias Naturales e IML, UNT, Miguel Lillo 205, CP 4000, San Miguel de Tucumán, Argentina
[b] Unidad Asociada de Petrología Experimental, CSIC-Universidad de Huelva, Campus El Carmen, 21071 Huelva, Spain
[c] Departamento de Geología, Universidad de Atacama, Copayapu 485, Copiapó, Chile

ARTICLE INFO

Article history:
Received 4 April 2013
Received in revised form 4 September 2013
Accepted 14 September 2013
Available online 22 October 2013

Handling Editor: Z.M. Zhang

Keywords:
Famatinian arc
Lower Ordovician
Cotectic trend
Sierra de Velasco batholith
Gondwana margin

ABSTRACT

The study of a magmatic series composed of Qtz-diorites to granites of the south part of the Sierra de Velasco batholith (Famatinian arc) in Argentina reveals that most rocks follow a coherent cotectic trend, which is comparable to a *cotectic line of liquids* (CLL) traced from experimental liquid compositions of calc-alkaline (andesitic) systems. The identification of cotectic relationships is crucial to interpret the meaning of geochemical variation trends in terms of phase equilibria. We show the contrast between typical CLL trends defined by rocks of the Palanche pluton and rocks departing from CLL array, which are interpreted as resulting from local processes of bulk assimilation of a pelitic host. Zircon U–Pb age determinations with SHRIMP support a coeval zircon crystallization record from of about 480 to 450 Ma of samples plotting on the CLL. The absence of intrusive contacts between these coeval cotectic granites implies that they were fractionated in situ at the level of emplacement. Other younger pulses (442 ± 5 Ma), also fall on the CLL, denoting that uniform processes of melting and fractionation were operative for at least 40 Ma at the same locus at the active continental margin of Gondwana. During this protracted magmatic activity, sporadic pulses of mafic magma were injected (e.g., at 456 ± 7 Ma), revealing a complex process of pulse amalgamation in the building up of the batholith. These mafic magma pulses may have contributed to basification of the host granitoid by enclave dissolution at the low pressure of emplacement. The reported geochemical trends, as true CLL, together with observed textures and crystallization sequences, point to a parental intermediate system of andesite composition (SiO_2 > 55 wt.%) with a water content of about 2.5 wt.% H_2O, similar to those formed by sediment–basalt subducted mélanges. A sublithospheric origin for the mafic precursor is proposed in agreement with prediction by recently published thermo-mechanical modeling and experimental phase equilibria.

1. Introduction

The Famatinian magmatic arc system in Northern Argentina represents the best preserved paleo-arc magmatic system of those formed at the margin of Gondwana during Ordovician. Particular geological setting, in relation to active tectonics and lithosphere duplication in Northern Argentina, has promoted fast crustal elevation and erosion leading to the surface large exposures of the innermost areas of this arc magmatic system (e.g., Otamendi et al., 2009a,b, 2012). Several Sierra alignments in the Pampean region of Northern Argentina are characterized by large exposures of granite batholiths that were mostly formed along the Paleozoic (Rapela et al., 1992; Pankhurst et al., 1998, 2000; Rossi et al., 2002). The Famatinian orographic system, with highs over 6000 m (General Belgrano peak is 6250 m high) and the Sierra de Velasco mountains (up to 4200 m), in Catamarca and La Rioja provinces, together with the Valle Fértil and La Huerta Mountains (2300 m) in San Juan province, offer an excellent geological laboratory to study deep-seated processes in the generation of arc magmatic systems. This study concerns with one of these large Paleozoic composite batholiths that were built at the Gondwana active margin in South America. It is denominated Sierra de Velasco batholith (from here SVB) and forms part of the Famatinian magmatic arc.

Lower Ordovician granites of calc-alkaline composition [I-type, according to the granite classification scheme of Chappell and White (1974)], almost identical to the Cordilleran batholiths formed during Mesozoic and Cenozoic along the America's active margin, are dominant in the Famatinian paleo arc (Saal et al., 1996; Toselli et al., 1996; Saavedra et al., 1998; Dahlquist et al., 2005; Otamendi et al., 2009a,b, 2012). However, other granites of S-type affinity (Toselli et al., 2000; Báez et al., 2005; Grosse and Sardi, 2005; Toselli et al., 2005; Grosse et al., 2009) and transitional terms between S- and I-type are also

* Corresponding author.
E-mail address: laurabellos@yahoo.com.ar (L.I. Bellos).

1342-937X/$ – see front matter
http://dx.doi.org/10.1016/j.gr.2013.09.019

present (Grosse et al., 2011). Continuous exposures along 100 s km of fresh rocks allow us to study deep-seated intrusions (e.g., Valle Fértil batholith or paleo arc; Pankhurst and Rapela, 1998; Pankhurst et al., 1998; Otamendi et al., 2009a,b, 2012; Castro et al., 2014) and to explore processes of magma evolution during crystallization in deep-seated magma chambers. Fundamental processes that are often invoked in granite petrogenesis on the basis of geochemical relations compared with expected results from models (e.g. magma mixing assimilation, crustal melting, etc.), can be tested by the study of detailed sections in these well-exposed batholiths.

A major problem about the generation of calc-alkaline batholiths in active continental margins concerns the high temperatures (>1000 °C) required to stabilize Ca- and Mg-rich silicic melts (63–70 wt.% SiO_2; 4–6 wt.% CaO; 1–3 wt.% MgO) at deep-crustal pressures (Castro et al., 2013). These temperatures exceed the maximum values predicted by thermal models even if advection by mantle-derived basalts is hypothetically considered in models (Annen et al., 2006). The crystallization history compared with phase equilibrium determinations for water-undersaturated systems is in accordance with low initial water contents (<2 wt.% H_2O) implying high temperatures (>1000 °C) measured on X_{H2O}-T sections (Maaloe and Wyllie, 1975; Naney, 1983). Two possible solutions are often invoked to skip the paradoxical implications mentioned above of calk-alkaline granite magma generation. The first solution is that magmas contained high water contents and, consequently they were liquid systems at moderate T of about 850 °C that are within realistic values in intracrustal thermal models (e.g., Bea et al., 2003; Bea, 2012) and are supported by mineral thermobarometry in lower crust granulite xenoliths (Castro et al., 2014 and references therein). The second solution is that calc-alkaline granites never were liquids but crystal-rich mushes in which the crystal fraction represents the solid residue (restites) from a partially molten crustal source, transported by restite entrainment (Clemens et al., 2011). In the latter case, the composition of the liquid fraction (ca. 50 vol.%) can be close to the granite minimum and, hence, can be stable at moderate T within the range of 650–850 °C, depending on the water content. Mafic minerals (biotite, hornblende, pyroxene, etc.) and Ca-rich plagioclase form the solid fraction that is assumed to be dragged from the source.

However, these two hypothetical solutions fail to account for the observed textural relations in calc-alkaline granitoids. First, they are characterized by water undersaturation and scarcity of pegmatites, as it is broadly recognized in Cordilleran batholiths (e.g., California: Presnall and Bateman, 1973; Patagonia: Castro et al., 2011), far from the water contents (>5 wt.%) required to set the system at its liquidus at deep crustal pressure. Initial water contents of about 5 wt.% will imply saturation at the pressure of emplacement (<200 MPa for most cordilleran-type batholiths) and early crystallization of hornblende as the system liquidus phase. Second, the common mafic minerals, namely biotite and amphibole, show textural relations of magmatic crystallization evidencing that Fe and Mg were components dissolved in the liquid and not transported by magmas as entrained restitic minerals. The implication is that water content reached the required value to stabilize hydrous minerals (4 wt.% water at 200 MPa; Naney, 1983) at late stages in the magmatic evolution, implying that the initial water content of the system was much lower and, hence, much hotter than expected if it is water-saturated at the liquidus.

Moreover, there are several arguments against granitoids as crystal mushes derived from an incompletely molten crustal source. Indirect arguments are, for instance, (1) the presence of volcanic equivalents (dacites and rhyolites) in which phenocrysts grew from a liquid system in a shallow magma chamber (Pichavant et al., 1988a,b; Pichavant and Macdonald, 2007) and (2) the formation of early chilled margins eroded and transported as autholiths (Paterson and Vernon, 1995; Bea, 2010). Direct support on high intrusion temperature has been supplied in the neighboring Ordovician Valle Fértil batholith (Castro et al., 2014), through the study of partially molten metagabbro inclusions in Qtz-diorites, recording values of T > 1000 °C in Opx-bearing trondhjemitic veins.

Consequently, the problem of calc-alkaline magma generation is mostly related to phase equilibria and thermal requirements. In case that these magmatic systems represent water-poor liquids, the temperatures will exceed any crustal thermal model and the intra-crustal origin of magmas can be seriously questioned (see Castro, 2013). Here we show ages and compositional relationships of a Cordilleran-type batholith from the Famatinian (Ordovician) arc system in South America. Relations are unambiguously related to crystallization from a liquid system. Some rock trends are identified as cotectic liquids that fairly follow *cotectic liquid lines* (CLL), which is not compatible with other possible magmatic evolution trends due to self-assimilation of cumulate crystals, crystal-melt suspensions or local contamination with country rocks.

Selected outcrops of the SVB have been studied for geochronology and whole rock geochemistry. The aim of this study is to present the whole petrology, geochemistry and the first precise geochronological data of the southern part of the Sierra de Velasco batholith, further more to decipher the complex geochemical and dynamical evolution of granitic magmas, the identification of cotectic and non-cotectic variations, among other processes leading to magma differentiation, and to test multi-pulse formation of batholiths (Coleman et al., 2004; Glazner et al., 2004; Paterson et al., 2011).

2. Geological setting

The SVB batholith is one of the several granite–tonalite batholiths that conform the Famatinian magmatic arc (Fig. 1), together with associated Lower Paleozoic volcanic and volcanoclastic sequences. The magmatic arc was built along the active proto-Andean margin of western Gondwana in response to the eastward subduction of a paleo-Pacific oceanic plate (e.g., Pankhurst and Rapela, 1998; Lucassen and Franz, 2005; Miller and Söllner, 2005; De los Hoyos et al., 2011). At the north branch of the arc, in the Puna and Famatinian System, Ordovician volcanic rocks are interbedded with sedimentary sequences (Toselli et al., 1990; Mannhein and Miller, 1996; Toselli et al., 1996; Pankhurst et al., 1998; Coira et al., 1999; Pankhurst et al., 2000; Cisterna, 2001; Viramonte et al., 2007), whereas in the south branch, deeper levels are exposed with granite–tonalite and associated basic rocks outcropping as large composite batholiths (Pankhurst et al., 2000; Murra and Baldo, 2006; Otamendi et al., 2009a,b, 2012; Castro et al., 2014).

Similar to other Cordilleran-type, magmatic arcs [e.g., the Mesozoic–Cenozoic Patagonian batholith (Pankhurst et al., 1999; Hervé et al., 2007; Castro et al., 2011)], the Famatinian arc is formed by batholiths of dominant calc-alkalic and calcic, I-type composition, with small bodies of peraluminous S-type plutons (granite types after Chappell and White (1974)) in the western part of the arc. Towards the east, the arc is characterized by the presence of dominant S-type plutons with transitional terms to typical I-type ones (Grosse et al., 2011). The Famatina System (Aceñolaza et al., 1996; Saavedra et al., 1998), the Ulapes–Los Llanos batholith (Pankhurst et al., 1998, 2000) and the Sierras de Valle Fértil–La Huerta (Otamendi et al., 2009a,b; Castro et al., 2014) form the metaluminous I-type belt, whereas Fiambalá, Capillitas, Zapata, part of Velasco and Mazán ranges (Toselli et al., 1996; Rossi et al., 2002) form the eastern belt of peraluminous granites.

The SVB is part of a mountain system called Sierras Pampeanas in Northwestern Argentina. The evolution of Sierras Pampeanas during the Upper Proterozoic and Paleozoic is characterized by two main periods of convergence along the proto-Pacific margin of Gondwana that generated two main orogenic cycles: the Pampean (~580–520 Ma) and Famatinian (~490–350 Ma) cycles (Aceñolaza and Toselli, 1981). Geologically, Sierras Pampeanas consist in a series of basement blocks that were exhumed during the Neogene by high-angle, N–S trending reverse faults (González Bonorino, 1950; Jordan

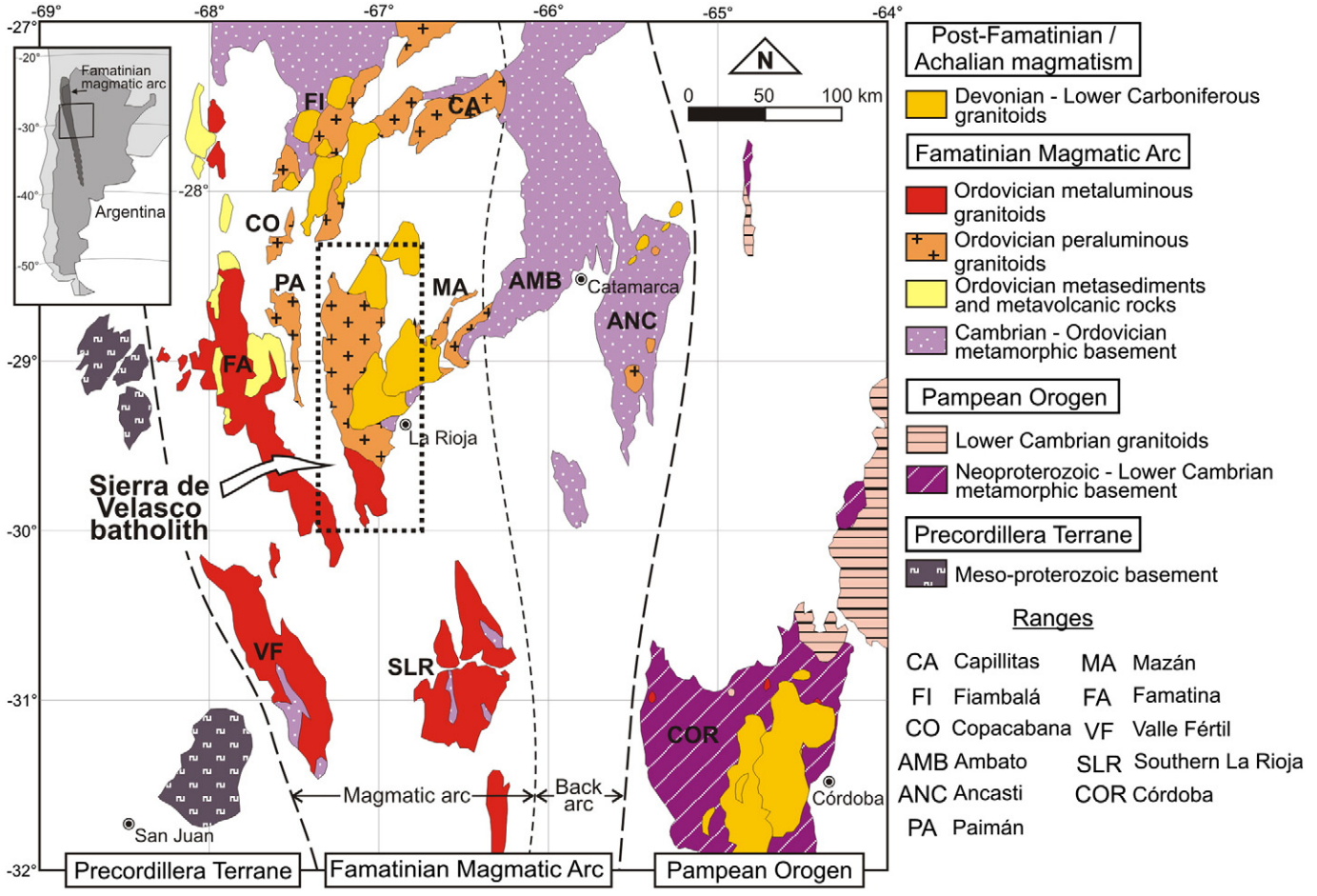

Fig. 1. General geological map of the central part of the Sierras Pampeanas of NW Argentina, modified from Grosse et al. (2011). Precordillera terrane, Famatinian magmatic arc and Pampean orogeny have been delimited. Dotted rectangle indicates location of Sierra de Velasco batholith as part of Famatinian magmatic arc.

and Allmendinger, 1986; Isacks, 1988). Metamorphic and intrusive rocks of Precambrian to Lower Carboniferous age form these blocks almost entirely. The SVB was considered until recently as consisting almost entirely by peraluminous granitic rocks of Early Ordovician age (e.g., Pankhurst et al., 2000). However, more recent studies in the Sierra have shown that it is conformed by numerous plutons with ages ranging from Ordovician to Early Carboniferous (see Báez and Basei, 2005; Dahlquist et al., 2006; Toselli et al., 2007; Grosse et al., 2009). Peraluminous, S-type granitic rocks crop out in the central and northern parts of the Sierra, whereas metaluminous, I-type granitoids form the southern part. The relations between S- and I-type plutons are among the most intriguing features of this Lower Ordovician magmatic system, where Grosse et al. (2011) recognized transitional I/S-type granitoids. The origin of I-type granites and the relations with transitional terms will be discussed in this paper.

3. The Sierra de Velasco batholith

The SVB is almost entirely composed of granite–tonalite rocks forming a large batholith of 180 km length, flanked by high-angle reverse faults (Fig. 2a). A pre-intrusion metamorphic basement is only locally represented by small outcrops of metasedimentary rocks along the eastern flank of the batholith. These metasedimentary rocks can be correlated with La Cébila Formation (González Bonorino, 1951) in the Sierra de Ambato, to the northeast. La Cébila Formation is essentially metapelitic and is formed by schists, phyllites and subordinated interbedded quartzites. The depositional age of this unit can be constrained between ~530 Ma, which corresponds to the youngest zircons dated by Finney et al. (2003) and Rapela et al. (2007), and ~480 Ma, corresponding to the oldest granitoids of the sierras of Velasco and Mazán.

Granitic rocks conform many deformed and undeformed bodies ranging in age from Early Ordovician to Lower Carboniferous. Early Ordovician granite intrusions are represented in the NW of the SVB by the Antinaco Orthogneiss (Toselli et al., 2000). Several U–Pb age determinations are available on Early Ordovician S-type granitoids in the SVB; De los Hoyos et al. (2009) report two ages (conventional U–Pb on monazite) for S-type granitoids from the central-eastern flank: 476.4 ± 1.5 Ma for a biotite–muscovite granitoid and 465 ± 12 for a biotite–cordierite granitoid (Table 1). In the south part of the Sierra (Fig. 2a), Grosse et al. (2011) recognize transitional I/S-type granitoids that consist of Bt, Bt + Ms and subordinate Bt + Ttn + Aln + Ep

Fig. 2. (a) General geological map of the Sierra de Velasco batholith. Dotted rectangle indicates location of the study area. Green triangles indicate location of previous geochronological data reported in Table 1, from De los Hoyos et al. (2011), Pankhurst et al. (2000), Höckenreiner et al. (2003), Grosse et al. (2009) and Dahlquist et al. (2006). (b) Geological map of the study area in southern sector of the Sierra de Velasco batholith. Location of new analyzed samples used in this study and the U–Pb SHRIMP ages obtained are shown. See text for details.

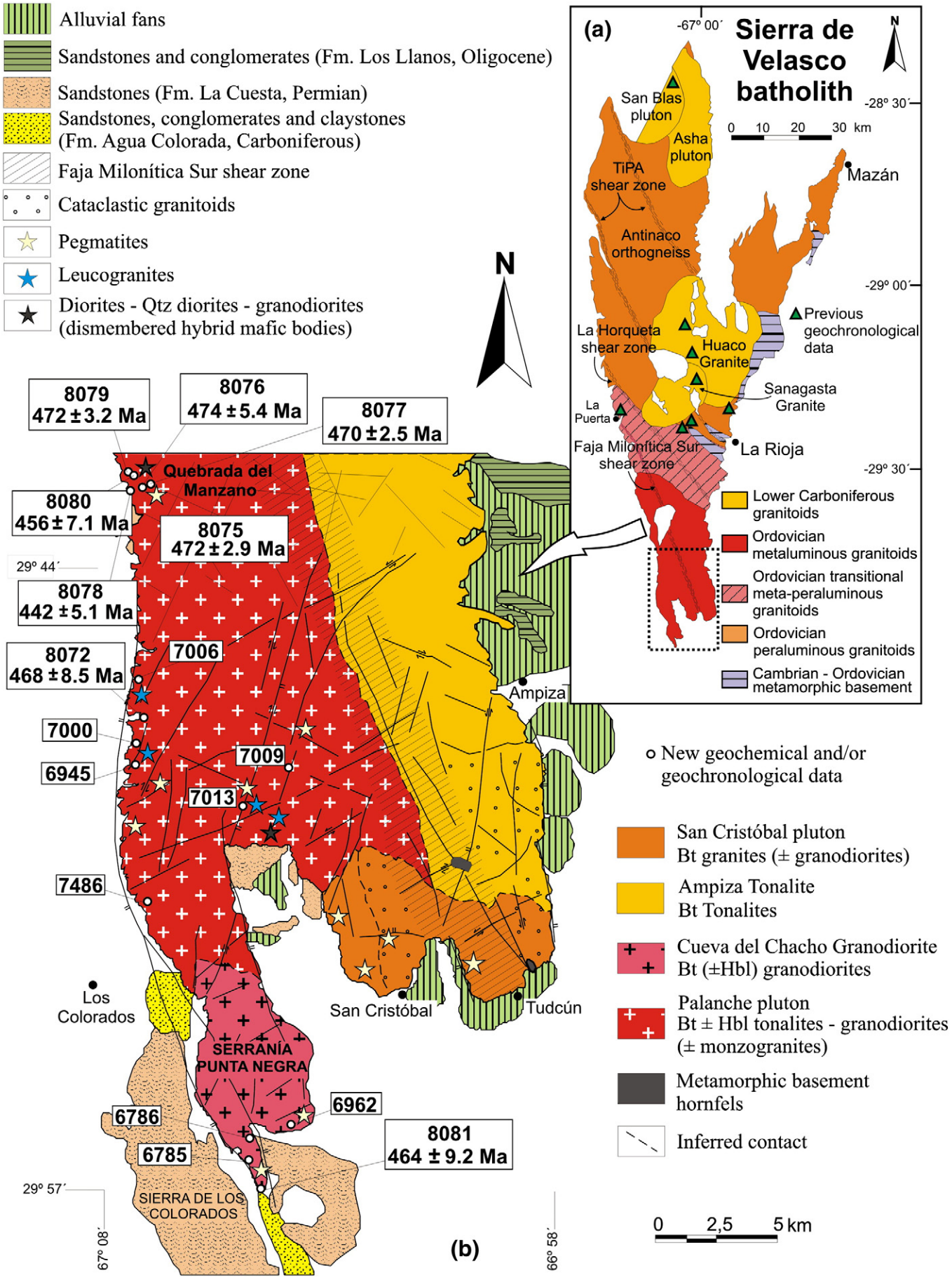
Alluvial fans
Sandstones and conglomerates (Fm. Los Llanos, Oligocene)
Sandstones (Fm. La Cuesta, Permian)
Sandstones, conglomerates and claystones (Fm. Agua Colorada, Carboniferous)
Faja Milonítica Sur shear zone
Cataclastic granitoids
Pegmatites
Leucogranites
Diorites - Qtz diorites - granodiorites (dismembered hybrid mafic bodies)
N
8079 472 ± 3.2 Ma
8076 474 ± 5.4 Ma
8077 470 ± 2.5 Ma
8080 456 ± 7.1 Ma
8075 472 ± 2.9 Ma
8078 442 ± 5.1 Ma
8072 468 ± 8.5 Ma
7006
7000
7009
6945
7013
7486
6962
6786
6785
8081 464 ± 9.2 Ma
Quebrada del Manzano
29° 44´
29° 57´
67° 08´
66° 58´
Ampiza
Los Colorados
San Cristóbal
Tudcún
SERRANÍA PUNTA NEGRA
SIERRA DE LOS COLORADOS
(b)
0 2,5 5 km
(a)
-67° 00´
Sierra de Velasco batholith
-28° 30´
-29° 00´
-29° 30´
0 10 20 30 km
San Blas pluton
Asha pluton
TiPA shear zone
Antinaco orthogneiss
Mazán
La Horqueta shear zone
Huaco Granite
Previous geochronological data
Sanagasta Granite
La Puerta
Faja Milonítica Sur shear zone
La Rioja
Lower Carboniferous granitoids
Ordovician metaluminous granitoids
Ordovician transitional meta-peraluminous granitoids
Ordovician peraluminous granitoids
Cambrian - Ordovician metamorphic basement
New geochemical and/or geochronological data
San Cristóbal pluton
Bt granites (± granodiorites)
Ampiza Tonalite
Bt Tonalites
Cueva del Chacho Granodiorite
Bt (±Hbl) granodiorites
Palanche pluton
Bt ± Hbl tonalites - granodiorites (± monzogranites)
Metamorphic basement hornfels
Inferred contact

Table 1
Previous geochronological data of Velasco batholith.

Area	Age (Ma)	Method	Rock	Ref.
La Rioja region	476.4 ± 1.5	Conventional U–Pb on Mnz	Bt + Ms granitoids	1
La Rioja region	465 ± 12	Conventional U–Pb on Mnz	Bt + Crd granitoids	1
La Puerta	481 ± 2.8	U–Pb SHRIMP on Zrn	Transitional I/S-type granitoids	2
La Rioja region	461 ± 11	Conventional U–Pb on Zrn	Transitional I/S-type granitoids	1
Copacabana range	402 ± 2	Sm–Nd on Grt	Mylonites (shear zone)	3
Sanagasta granite	352.7 ± 1.4	Conventional U–Pb on Mnz	Bt ± Ms ± Ttn ± Aln porphiric granites	4
Huaco granite	350 ± 5	Conventional U–Pb on Mnz	Bt + Ms porphiric granites	4
Huaco granite	358 ± 5	Conventional U–Pb on Mnz	Bt + Ms porphiric granites	4
San Blas pluton	340 ± 3	U–Pb SHRIMP on Zrn	Bt + Ms porphiric granites	5

Data sources: 1. De Los Hoyos et al. (2011), 2. Pankhurst et al. (2000), 3. Höckenreiner et al. (2003), 4. Grosse et al. (2009), and 5. Dahlquist et al. (2006). For localization of samples see Fig. 2a.

moderately peraluminous monzogranites, granodiorites and tonalites (abbreviations minerals after Kretz (1983)). Two ages have been determined for these rocks: 481 ± 3 Ma (U–Pb SHRIMP on zircon) by Pankhurst et al. (2000) and 461 ± 11 Ma (conventional U–Pb on zircon) by De los Hoyos et al. (2009). The Early Ordovician granitoids are cut by numerous NNW–SSE trending shear zones, which also affect other ranges further to the north (e.g. Höckenreiner et al., 2003; López et al., 2006). These shear zones consist of gneissic granites, cataclasites, protomylonites and mylonites (Durand and López, 1996). The shear zones of the SVB have not been dated. However, age determinations have been performed on similar mylonites located in the Sierra de Copacabana that are a continuation of the Velasco shear zones; Höckenreiner et al. (2003) dated syntectonically grown garnets from mylonites and obtained an age of 402.0 ± 2.0 Ma by the Sm–Nd method. Lower Carboniferous magmatism in the SVB is represented by several plutons in the central-eastern and northern sectors of the Sierra. These post-tectonic Lower Carboniferous granites intruded Ordovician granitoids (Antinaco Orthogneiss) and cross-cut the shear zones (e.g., Dahlquist et al., 2006; Grosse et al., 2009; Dahlquist et al., 2010; Fig. 2a; Table 1). They are high-K, peraluminous, porphyritic syeno- and monzogranites related with a post-orogenic to anorogenic setting (Grosse et al., 2011).

Granitoids of the south branch of SVB were described by Bellos (2005). These are dominantly Bt–Hbl-bearing granodiorites and tonalites and subordinated Bt-bearing monzogranites. They contain mafic enclaves and synplutonic dykes. These rocks are well exposed at the southern tip of the SVB, forming the Palanche pluton (Fig. 2b) and constitute the main focus of this petrologic/geochronologic study. The southern tip of the SVB is constituted by four granitic bodies, namely Ampiza tonalite, Cueva del Chacho granodiorite, San Cristóbal granite and Palanche pluton (Bellos et al., 2010; Fig. 2b).

Host rocks to batholith intrusion are very scarce. The plutons contain xenoliths (2 to 50 cm length) of fine grained (metasedimentary) rocks formed by Qtz, Kfs and Bt. In particular, the San Cristóbal granite contains quartzite xenoliths and small hornfels blocks with the characteristic metamorphic assemblage Qtz, Kfs, Bt, Cord, Sill. These metamorphic rocks originated from psamo-pelitic sediments of the La Cébila Formation.

4. Analytical techniques

In this paper we describe the four granitic bodies that constitute the south part of the SVB, focusing on the Palanche pluton the main sampling for the geochemical and geochronological study, and field work in order to explore the intrusive relations (Fig. 2b). The aim of this sampling was to have a complete trend of rocks, from the most mafic units to the more felsic ones. Knowing the coupling or decoupling between ages and magmatic processes is essential to decipher the complex process of batholith generation and the potential implication on large scale processes of new crust generation at active continental margins.

4.1. Whole rock and microprobe analyses

18 samples were analyzed at the universities of Oviedo and Huelva (Spain) by XRF and ICP-MS respectively. At Oviedo, major elements and Zr were analyzed by X-ray fluorescence (XRF) using glass beads. The precision of the XRF technique is better than ±1.5% relative. At Huelva, trace elements, including rare earth elements (REE), were analyzed by inductively coupled plasma mass spectrometry (ICP-MS) with an HP-4500 system, following digestion in an HF + HNO_3 (8:3) solution, drying and further second dissolution in 3 ml HNO_3. The average precision and accuracy for most of the elements were determined by repeated analyses of the SARM-1 (granite) and SARM-4 (norite) international rock standards, and are in the range 5–10% relative. Mineral analyses were performed by electron microprobe analyses with a JEOL JXA-8200 SuperProbe and by EDS in a SEM, at the University of Huelva (Appendix A). In both cases a combination of silicates and oxides was used for calibration.

4.2. U–Pb SHRIMP zircon analyses

Eight samples were selected for geochronological studies. Samples 8072, 8076, 8078, 8079, 8080 and 8081 were analyzed in a SHRIMP II machine at the Chinese Academy of Geological Sciences (Beijing SHRIMP Center), and samples 8075 and 8077 were analyzed in the SHRIMP IIe/mc at the IBERSIMS Lab (University of Granada, Spain). Zircon separation was accomplished at the University of Huelva by traditional techniques using dense liquids and magnetic (Franz) separation. Selected crystals free of impurities and fractures were selected by handpicking with a binocular lens. Analytical procedures from both SHRIMP labs are described in Appendix B.

5. Intrusive units: field relations and petrography

In order to follow a systematic description, the rocks were initially classified by field and petrographic criteria based on Kfs content and mafic mineralogy. Subsequently, this provisional classification was corrected using chemical and mineralogical criteria that in general terms follow the QAP classification scheme. According to the Frost et al. (2001) classification scheme, the intrusive units are of magnesian-type and evolve along a typical calc-alkalic series (Fig. 3). According to a combination of chemical and mineralogical criteria, together with field relations, four intrusive units have been distinguished (Fig. 2b). As mentioned above, these are (1) the Ampiza tonalite, (2) the Cueva del Chacho granodiorite, (3) the San Cristóbal granite and (4) the Palanche pluton. Mafic igneous rocks present in the Palanche pluton and San Cristóbal granite are described separately.

5.1. Ampiza tonalite

The Ampiza tonalite has been described in the southeastern flank of the SVB. It had preliminary been considered as a facies of the Palanche

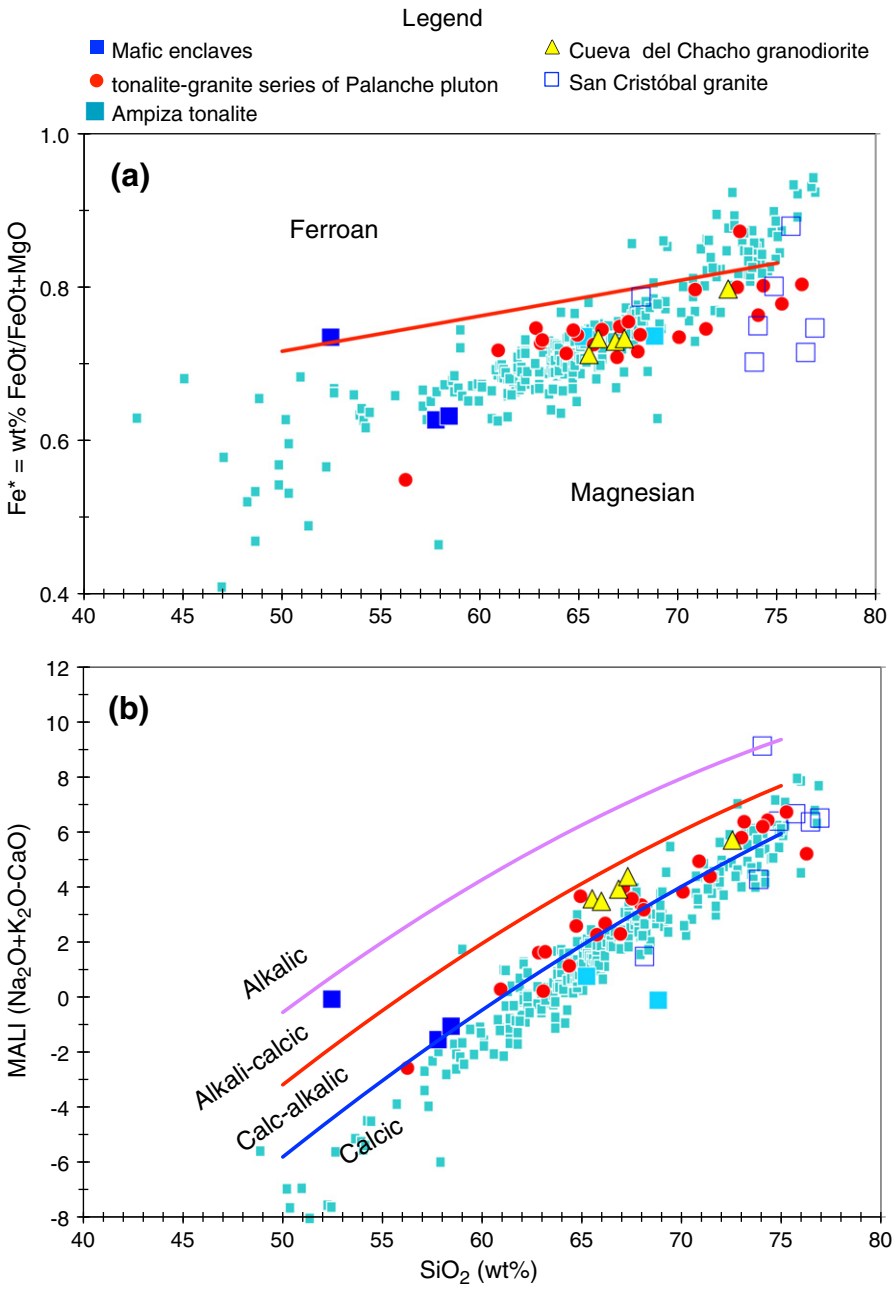

Fig. 3. Granitoids classification diagrams (Frost et al., 2001). Light blue squares in the background are data from Peninsular Range batholith in North America after Lee et al. (2007).

pluton (Bellos, 2005), but its petrographic and geochemical features strongly suggest that it is a different plutonic body. The contacts with the Palanche pluton and San Cristóbal granite are inferred in the maps (Fig. 2). They are dark gray, equigranular and medium-grained tonalites. The mineral assemblage is Pl + Qtz + Bt + Ap ± Kfs ± Aln. They are characterized dominantly by the presence of Bt, together with prismatic allanite of up to 1.5 mm, surrounded by a mantle of epidote.

5.2. Cueva del Chacho granodiorite

These rocks outcrop in the SW tip of the SVB (Fig. 2). This intrusive body had been considered, like the Ampiza tonalite, as a facies of the Palanche pluton. They are pinkish-gray, porphyritic with 15–20 vol.% of reddish microcline megacrysts of up to 2–3 cm. To the north the percentage of megacrysts decreases and the contact with the Palanche pluton appears to be transitional. Granodiorites are medium to coarse-grained, xenomorphic to hypidiomorphic with the dominant association of Qtz + Pl (andesine) + Kfs (microcline) + Bt + Amp + Ttn + Ap + Zrn + Mag ± Aln.

Some crystals have signs of solid state deformation such as ondulouse extinction in Qtz, feldspars with deformed twins and kink folds and myrmekites in the Kfs–Pl contact. Biotite has Mg-number average of 0.50 and Al^{IV} ranging between 2.49 and 2.63 a.p.f.u. (atoms per formula unit). It is classified as eastonite mainly. Biotite is associated with opaque minerals. Titanite and brown prismatic Aln, sometimes surrounded by a

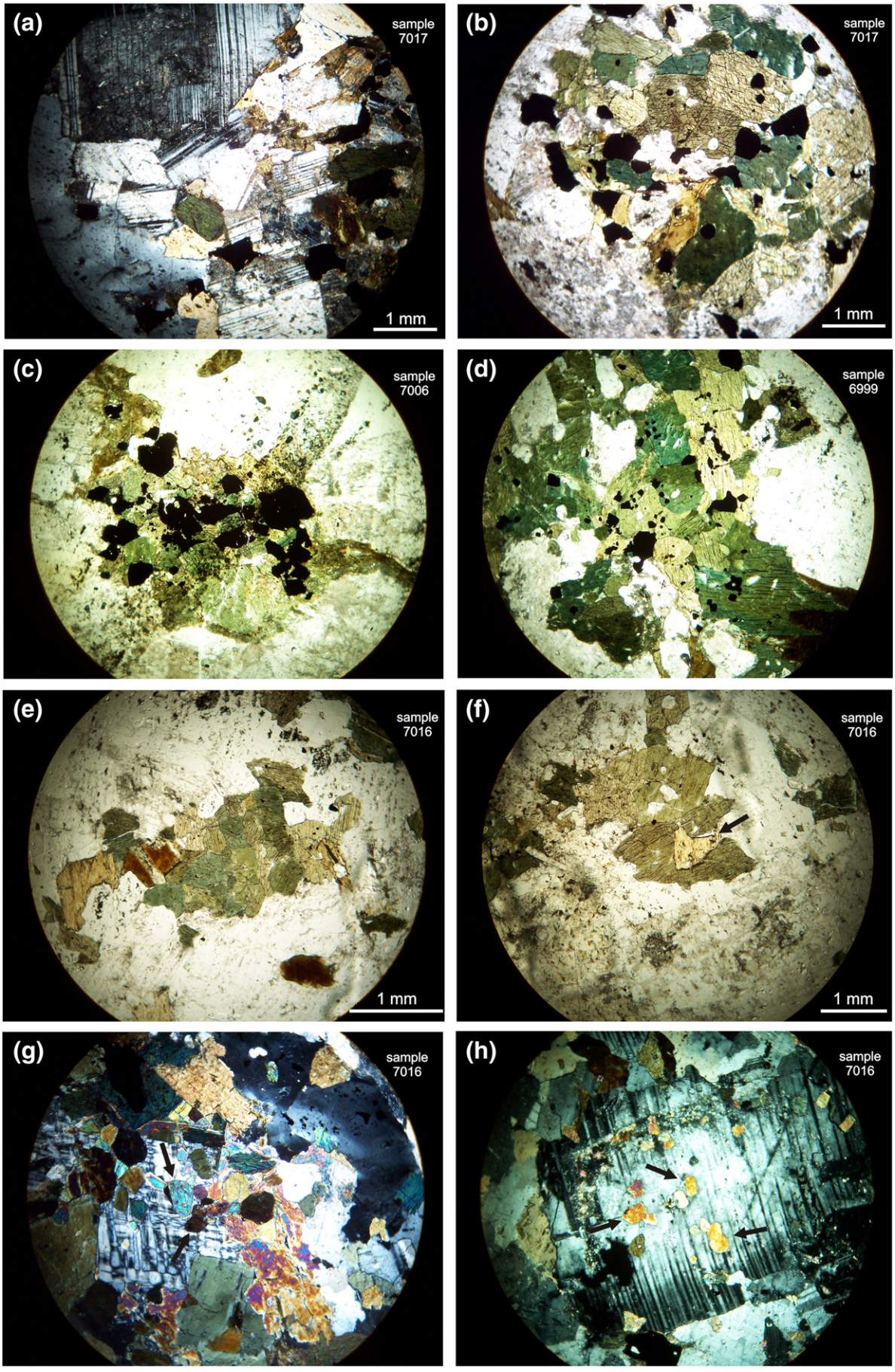
(a)
sample 7017
1 mm
(b)
sample 7017
1 mm
(c)
sample 7006
(d)
sample 6999
(e)
sample 7016
1 mm
(f)
sample 7016
1 mm
(g)
sample 7016
(h)
sample 7016

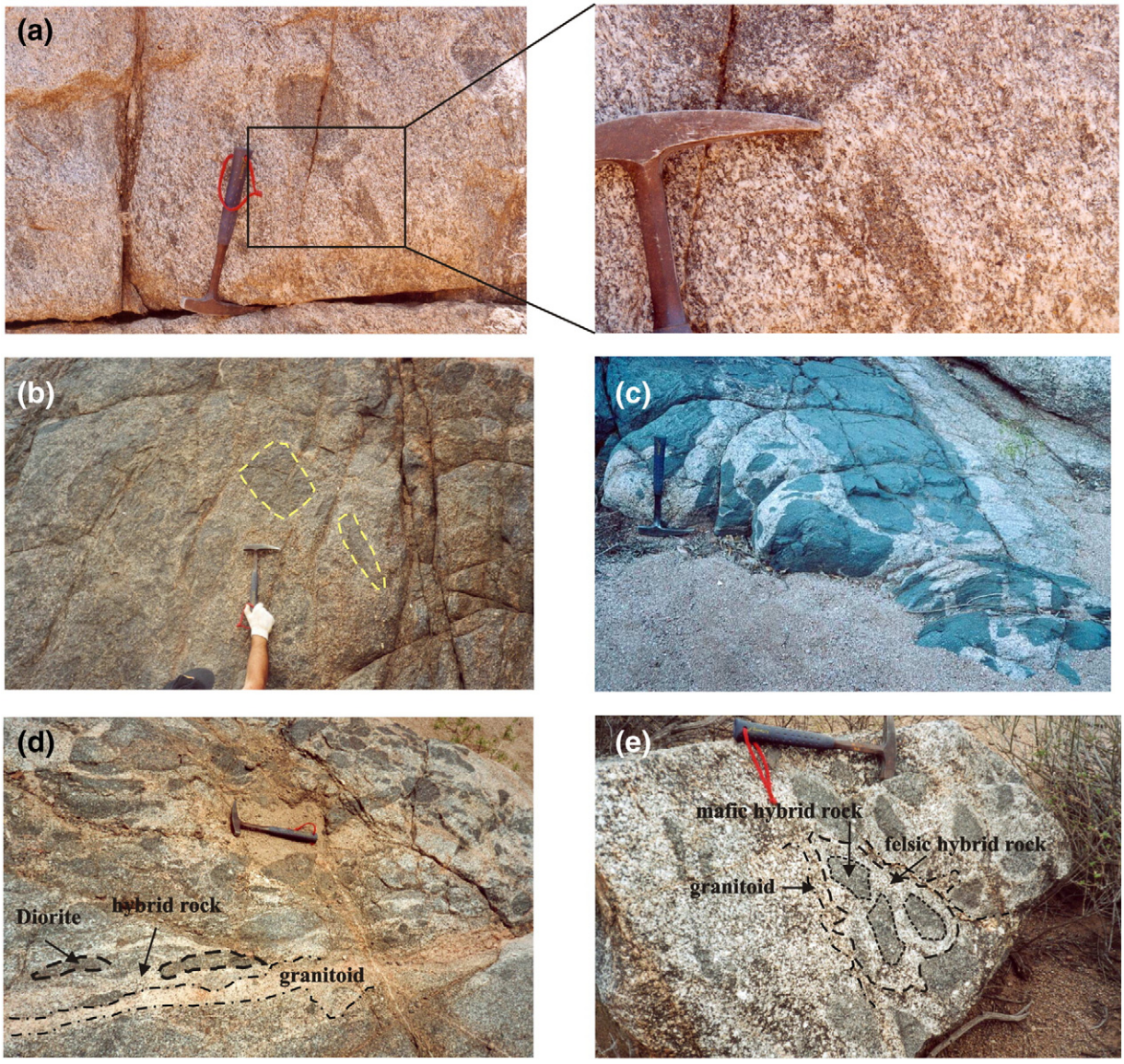

Fig. 5. Field relations of granitoids from Palanche pluton and the mafic rocks (a) magmatic enclave digested by the granitoid; (b) and (c) dismembered mafic bodies in the Palanche pluton; (d) and (f) mingling between mafic rocks and the host granitoid, generating rocks with different degrees of hybridization.

mantle of pistacite, are associated with Bt. A feature of this facies is that the Amp is very scarce and is only found occasionally as small irregular and dismembered crystals.

5.3. San Cristóbal granite

It is a granitic body that covers an area of 35 km^2 at the southeastern tip of the batholith (Fig. 2). Its contact with the Palanche pluton is inferred. It consists of equigranular to slightly porphyritic Bt-monzogranites, syenogranites and subordinate granodiorites. The mineral assemblage of this pluton is Kfs (microcline) + Pl (oligoclase–andesine) + Qtz + Bt + Mag ± Ms ± Grt. The granites are calc-alkaline, weakly- to moderately peraluminous. Zones of the San Cristóbal granite, Palanche pluton and the Ampiza tonalite were affected by shear zones that formed the Southern shear-zone (*Faja Milonítica Sur*), which has a NNW–SSE strike and extends from the southeast of the batholith towards the northwest beyond the study area. The shear zone consists of mylonites and protomylonites, with minor superimposed cataclasites (López et al., 2006; Bellos et al., 2010).

5.4. Palanche pluton

The Palanche pluton covers an area of ca. 200 km^2, extending towards the north, beyond the study area (Fig. 2). It consists of biotite–hornblende granodiorites and tonalites, together with minor biotite-monzogranites. Two textural facies have been recognized: one is equigranular and the other is slightly porphyritic. Mineral associations are very similar in both facies, although with modal variations. In the central part of the pluton,

Fig. 4. Photomicrographs from samples of Palanche pluton, (a) plagioclase cumulates in granodiorite; (b) hornblende cumulates in granodiorite; (c) and (d) hornblende and magnetite clusters; (e) hornblende cluster in granodiorite; (f) inclusion of biotite in hornblende in granodiorite; (g) euhedral crystals of hornblende included in microcline in granodiorite; and (h) euhedral crystals of hornblende included in plagioclase in granodiorite.

Table 2
Major (wt.%) and trace element (ppm) composition of representative samples from the Velasco batholith.

Location	Palanche pluton								Palanche (leucogranites)				Cueva del Chacho granodiorite				Palanche (enclaves)	
Sample ref.	7006	6945	7486	8072*	8078*	8079*	8075*	8076*	6951	7000	7009	7013	6785	6786	6962	8081*	8080*	8077*
Rock type	Tn	Grd	Pph Gr	Tn	Grd	Mz	Gr	Mz	Mz	Sy	Mz	Mz	Pph Grd	Pph Grd	Grd	Pph Gr	Hy	Tn
SiO_2	65.72	66.14	71.39	63.04	68.07	66.90	64.34	76.23	75.22	74.03	70.84	73.1	67.27	65.95	72.51	67.95	58.42	74.28
TiO_2	0.67	0.64	0.41	0.48	0.55	0.60	0.74	0.23	0.20	0.24	0.45	0.22	0.56	0.69	0.32	0.60	0.90	0.21
Al_2O_3	15.77	15.43	14.27	17.23	14.76	15.07	16.19	12.34	13.10	13.30	13.91	13.66	14.95	15.38	13.8	14.97	16.70	13.20
FeOt	4.30	3.99	2.40	4.57	3.57	3.91	4.80	1.47	1.25	1.49	2.97	2.04	3.50	4.45	2.09	3.65	6.22	1.21
MgO	1.63	1.37	0.82	1.72	1.27	1.61	1.93	0.36	0.36	0.46	0.76	0.30	1.28	1.63	0.53	1.45	3.63	0.30
MnO	0.13	0.09	0.06	0.28	0.13	0.08	0.11	0.04	0.03	0.04	0.09	0.02	0.08	0.12	0.04	0.10	0.15	0.04
CaO	4.25	3.85	2.69	5.30	3.12	3.71	4.20	1.57	1.38	1.62	2.40	1.27	2.81	3.22	1.93	3.07	6.23	1.43
Na_2O	3.38	3.16	3.07	4.55	2.49	2.31	2.77	1.82	2.70	2.66	2.94	2.63	3.15	3.30	2.65	2.54	2.46	2.09
K_2O	3.16	3.39	4.02	0.98	3.82	3.71	2.58	4.97	5.42	5.17	4.41	5.03	4.06	3.42	4.99	3.89	2.73	5.78
P_2O_5	0.20	0.17	0.10	0.24	0.15	0.17	0.24	0.06	0.04	0.06	0.10	0.07	0.15	0.19	0.08	0.16	0.26	0.05
Loi	0.68	0.42	0.70	0.48	0.74	0.92	1.14	0.44	0.32	0.57	0.46	1.56	0.76	0.93	0.82	0.66	1.03	0.62
Total	100.4	99.09	100.2	98.86	98.67	98.99	99.04	99.53	100.2	99.79	99.64	100.1	98.94	99.75	99.99	99.03	98.73	99.20
Mg#[a]	0.40	0.38	0.38	0.40	0.39	0.42	0.42	0.30	0.34	0.36	0.31	0.21	0.39	0.39	0.31	0.41	0,51	0,31
ASI[b]	0.94	0.97	1.00	0.95	1.06	1.03	1.08	1.10	1.02	1.03	1.00	1.13	1.02	1.02	1.04	1.07	0.91	1.07
Trace elements																		
Li	19.92	22.79	20.05	11.50	22.21	16.00	11.69	14.19	17.45	14.22	19.51	25.23	36.27	19.88	32.67	20.30	21.82	39.09
Be	2.71	3.43	2.24	3.77	1.69	1.65	1.16	1.15	2.40	2.48	1.72	2.16	12.75	2.95	2.40	1.88	1.73	1.88
Sc	16.10	13.01	6.98	107.3	12.68	10.05	2.37	1.94	1.63	2.34	7.48	2.01	7.23	8.90	2.88	9.65	20.80	13.37
V	95.04	83.65	44.54	92.90	61.31	79.90	18.83	18.86	17.54	25.14	26.95	30.76	76.45	56.88	42.90	59.93	147.3	70.71
Cr	69.85	58.85	30.76	27.41	39.24	23.79	27.84	13.80	43.40	52.22	48.32	73.14	24.94	12.14	33.01	20.85	75.27	32.08
Co	27.40	28.70	21.80	24.14	20.94	20.82	30.59	24.35	29.14	28.72	20.88	22.44	44.26	21.34	29.87	22.48	26.48	28.28
Ni	13.83	9.83	10.04	10.92	8.32	11.79	9.68	8.10	8.61	12.91	6.91	10.15	11.85	8.07	10.68	7.47	34.52	15.71
Cu	13.33	10.87	4.82	23.34	7.21	12.18	3.15	2.92	3.01	3.66	2.75	4.60	6.66	4.55	5.10	8.36	19.21	16.59
Zn	65.70	61.48	41.10	74.19	48.32	45.26	20.49	25.97	23.44	28.65	62.24	24.81	53.36	46.01	28.33	46.10	66.54	54.43
Ga	35.66	50.64	41.03	20.41	13.44	13.14	12.27	9.92	27.79	29.25	28.88	34.39	53.27	29.64	47.22	13.06	14.99	16.60
Rb	92.84	119.6	115.6	38.14	86.07	74.29	123.09	90.75	124.9	166.7	88.72	156.5	128.1	69.35	159.8	108.2	73.81	110.3
Sr	148.2	176	143.8	125.6	129.1	133.7	90.86	91.36	82.41	122.7	107.9	91.2	149.2	110.1	116.7	154.9	163.9	157.1
Y	41.24	24.66	22.97	144.3	44.68	24.91	8.96	7.43	3.49	19.70	14.66	9.37	14.63	17.65	11.43	18.27	17.33	21.66
Zr	65.51	54.09	41.25	94.75	58.13	58.95	224.7	44.03	68.97	40.4	41.09	84.86	50.44	38.53	63.8	58.49	55.65	110.1
Nb	17.90	12.82	12.55	19.89	13.25	9.41	3.48	4.46	2.70	9.54	8.10	4.28	12.22	8.66	6.02	7.67	8.53	8.16
Cs	2.58	4.50	2.85	1.53	2.47	2.38	1.62	2.69	2.92	2.89	2.28	9.05	3.37	2.51	5.31	3.10	1.77	4.23
Ba	592	887.7	841.2	79.71	848.8	749.6	467.9	558.9	433.3	525.4	517.7	583.9	957.4	618.2	1012	1015	576.1	404.5
La	31.51	49.61	47.27	30.59	39.53	34.94	28.80	46.91	38.78	26.30	43.17	38.96	45.80	27.48	45.57	47.66	31.55	36.89
Ce	75.65	93.93	92.50	83.85	91.31	72.12	57.39	86.29	69.85	51.66	81.38	68.17	87.33	57.15	78.83	95.13	66.24	71.67
Pr	10.93	12.05	12.23	12.99	10.81	8.06	5.73	8.48	7.74	6.45	9.82	7.50	9.74	7.45	9.08	9.88	7.47	7.63
Nd	41.41	43.53	42.82	62.57	42.63	31.04	19.33	27.47	23.55	22.94	35.21	23.66	30.70	27.25	29.13	35.36	28.83	27.87
Sm	8.85	7.93	7.23	21.04	9.49	6.41	2.76	3.61	2.72	4.41	5.61	3.08	4.21	5.14	4.13	5.90	5.44	5.13
Eu	1.94	1.95	1.73	1.27	1.46	1.39	0.75	1.05	0.91	1.05	1.30	0.69	1.39	1.22	1.35	1.47	1.44	1.42
Gd	8.70	6.99	5.87	19.79	8.06	5.39	1.95	2.35	1.67	3.99	4.71	2.30	3.38	4.53	3.11	4.60	4.37	4.40
Tb	1.46	1.03	0.87	3.36	1.23	0.83	0.27	0.31	0.18	0.66	0.66	0.29	0.47	0.68	0.40	0.63	0.64	0.65
Dy	8.62	5.46	4.63	24.38	7.71	4.77	1.42	1.53	0.70	3.73	3.50	1.52	2.54	3.69	2.03	3.26	3.46	3.60
Ho	1.86	1.10	0.96	5.23	1.63	0.99	0.26	0.27	0.14	0.82	0.66	0.33	0.57	0.78	0.43	0.70	0.71	0.77
Er	5.09	2.83	2.66	13.21	4.22	2.55	0.81	0.75	0.40	2.29	1.70	0.98	1.67	2.09	1.26	2.01	1.89	2.05
Tm	0.72	0.40	0.41	1.58	0.56	0.38	0.13	0.13	0.08	0.36	0.22	0.15	0.30	0.29	0.21	0.34	0.30	0.31
Yb	3.77	2.30	2.57	8.57	3.49	2.30	0.77	0.86	0.50	2.26	1.26	1.06	2.25	1.61	1.41	2.10	1.86	1.92
Lu	0.59	0.36	0.43	1.21	0.51	0.35	0.14	0.14	0.12	0.37	0.18	0.20	0.44	0.25	0.25	0.36	0.29	0.27
Ta	2.52	2.31	2.42	2.32	2.05	1.61	2.93	1.80	2.22	2.99	1.51	1.74	3.29	1.81	2.47	2.09	1.45	2.17
W	158.8	166.9	151.2	n.a.	n.a.	n.a.	n.a.	n.a.	121.6	164.2	130.6	131.4	241.3	133.3	178	n.a.	n.a.	n.a.
Hf	n.a.	n.a.	n.a.	2.17	0.90	1.05	1.14	0.60	n.a.	n.a.	n.a.	n.a.	n.a.	n.a.	n.a.	0.98	0.90	0.83
Pb	18.91	17.78	20.76	15.78	16.68	15.04	23.25	18.25	26.67	32.65	18.50	23.22	21.26	11.33	21.38	16.19	10.03	11.69
Th	13.39	19.91	21.45	8.14	10.15	9.58	25.72	13.12	18.81	28.95	17.91	26.09	30.38	11.06	17.86	13.85	5.14	9.18
U	3.48	3.90	3.81	1.29	1.29	1.58	1.38	1.62	1.88	3.65	1.26	1.71	3.01	2.37	1.90	2.10	0.82	0.98

Tn: Tonalite, Gr: Granite, Grd: Granodiorite, Mz: Monzogranite, Sy: Syenogranite, Hy: Hybrid mafic rock, Pph: Porphiric, n.a.: not analyzed.
[a] Mg# = Mol MgO / (MgO + FeO).
[b] ASI = Mol Al_2O_3 / (Na_2O + K_2O + CaO).
* Samples selected for geochronological study.

the rocks are porphyritic granodiorites, whereas in the western flank equigranular tonalites dominate with minor proportion of granodiorites. Monzogranites are scarce and they are associated to granodiorites in the central part of the pluton. Porphyritic granodiorites are pinkish gray to white-gray, with pale-pink to white microcline megacryts (5–10 vol.%) of up to 1.5 cm. The percentage of megacrysts decreases towards the western flank to values below 5 vol.%, becoming the composition predominantly tonalitic. The rocks are normally hypidiomorphic, medium grained with the dominant association of Qtz + Pl + Kfs + Bt + Amp. Accessory phases are Ttn, Aln, Ap, Zrn, Mag, Py and Rt. Some crystals have signs of solid state deformation such as ondulouse extinction in Qtz and Pl with incomplete twins and kink folds. Early cumulates of Pl are present in some samples (Fig. 4a), with composition ranging from An_{26} to An_{51} with an average of An_{38}. In the tonalites, Kfs (microcline) is absent or interstitial, whereas in the more acid rocks it occurs as poikilitic crystals with deformed twins, myrmekites and fine pertites and may have inclusions of Pl and Amp. Biotite and Amp occur as cluster

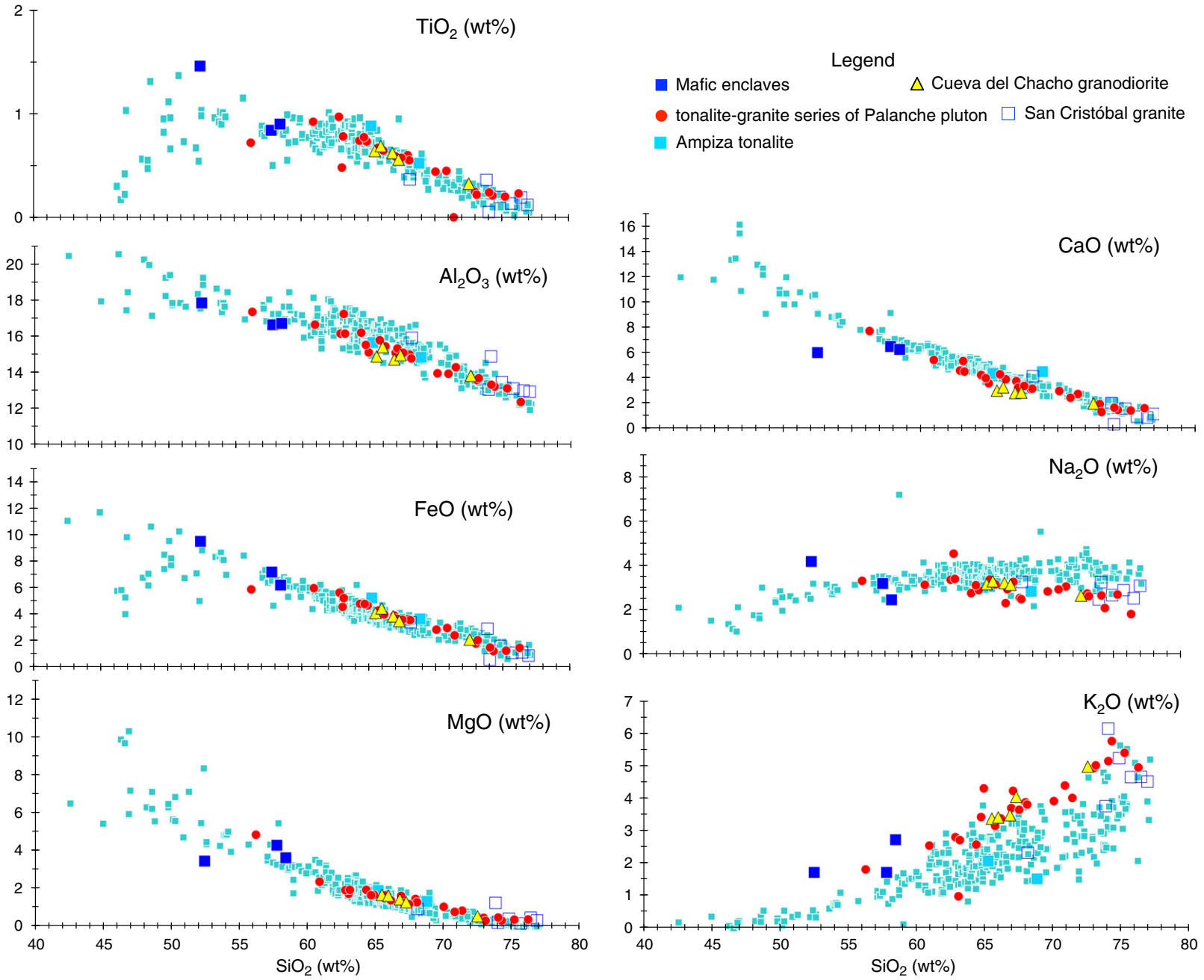

Fig. 6. Silica variation diagrams (Harker) plotting granitoids and mafic enclaves of the southern part of the Sierra de Velasco batholith. Light blue squares in the background are data from Peninsular Range batholith in North America after Lee et al. (2007).

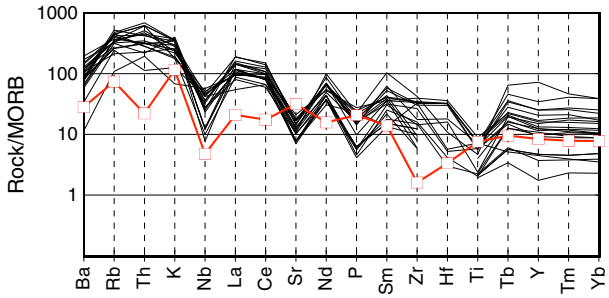

Fig. 7. Thompson normalization plot rock/MORB. The red line is the averaged values given by Kelemen et al. (2003) for typical continental arc andesites. In general, all samples of the calc-alkaline series of the Sierra de Velasco batholith show the typical depletion in Nb and Ti and enrichment in Ba, Rb, Th and K that characterize arc setting magmatism.

together with Mag (Fig. 4b–e). Biotite has Mg-numbers varying from 0.45 to 0.56 and Al^{IV} ranging between 1.49 and 2.90 a.p.f.u. (atoms per formula unit). Biotite is occasionally included in Amp (Fig. 4f).

Intrusive stocks and dykes of leucogranites have been recognized in the Palanche pluton. They are white to redish, medium-grained, leucocratic rocks with the mineral assemblage Qtz, perthitic Kfs, Pl, Bt (siderophyllite), Zrn and Ap.

5.5. Mafic igneous rocks

Mafic igneous rocks are present in the Palanche pluton and San Cristobal granite as isolated magmatic enclaves, dismembered bodies showing mingling relationships and late dykes. Diorite, Qtz-diorite and tonalite compositions are dominant. Magmatic enclaves are ovoid, ranging in size from several centimeters to one meter. Contacts with the host granitoid can be either sharp or diffuse, occasionally connected to Bt schlieren. They are dark gray with equigranular texture (Fig. 5a).

As it is reported in many calc-alkaline plutons, the same mineral association is present in enclaves and host granitoid, but in different proportions (e.g., Zorpi et al., 1989; Tepper and Kuehner, 2004; Barbarin, 2005). The common mineral association is Pl (andesine) + Qtz + Bt + Ttn + Ap + Zrn ± Kfs (as myrmekites) ± Amp. Plagioclase is present in two populations of different size. The larger crystals show a

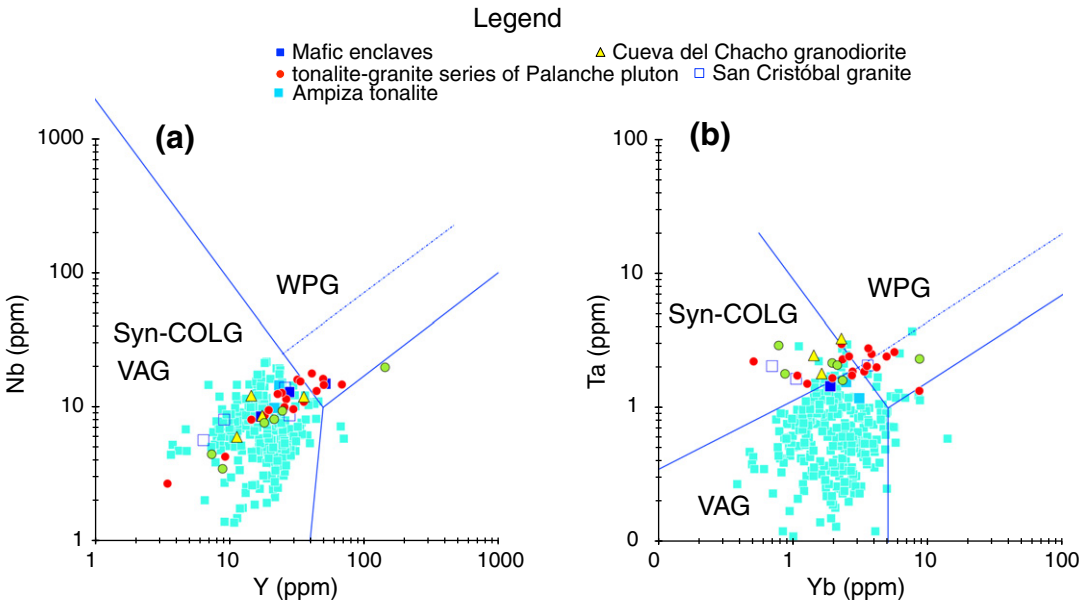

Fig. 8. Tectonic discrimination diagrams (Pearce et al., 1984). Green circles are the dated samples of the Palanche pluton. Light blue squares in the background are data from Peninsular Range batholith in North America after Lee et al. (2007).

Amphibole occurs in variable proportions and is absent in monzogranites. It is classified (Leake et al., 1997) as magnesio-hornblende and tschermakite and occasionally as edenite. The Mg-number varies from 0.47 to 0.67 and Si between 6.36 and 6.72 (a.p.f.u.). Amphibole is subhedral to anhedral. Amphibole may occur as inclusions in Pl and Mc (Fig. 4g, h). Zircon and apatite occur as inclusions in Bt and Amp. Opaque minerals (Mag and Py) and Ttn are associated with Amp and Bt. Allanite is occasionally present.

subhedral habit and have an internal ring, which is rich in inclusions. Quartz is generally interstitial, but it is also found as large embayed xenocrysts with corroded edges, surrounded by Amp in coronitic textures. Biotite is always present whereas Amp is more variable and forms clots. Titanite is associated with these mafic minerals. The elongated shape and the absence of textural evidence of deformation in the solid state in the enclaves suggests that they were deformed by magmatic flow (Vernon et al., 1988). Diffuse contacts, coronitic textures

Fig. 9. Chondrite-normalized (Sun and McDonough, 1989) REE plots. The Palanche pluton shows negative Eu anomaly, compatible with feldspar fractionation. The leucogranites have negative Eu anomaly, and a strong fractionation of REE, with exception of one of them, which has positive anomaly and a higher LREE/HREE fractionation. The patterns for LREE are similar to the other granitoids, but are more depleted in HREE. Samples of the Ampiza tonalite have variable negative Eu anomalies and a strong fractionation of the LREE in one of the samples. The Cueva del Chacho granodiorites have both positive and negative Eu anomaly. Two samples of San Cristóbal granite show negative Eu anomaly and another one shows positive anomaly. The three samples show similar patterns of LREE but one of them shows a low LREE/HREE fractionation. In general, the San Cristóbal granite is more depleted in REE than the Palanche pluton, but the patterns are very similar with gentle slopes of the LREE, and flat patterns of the HREE. See text for further details.

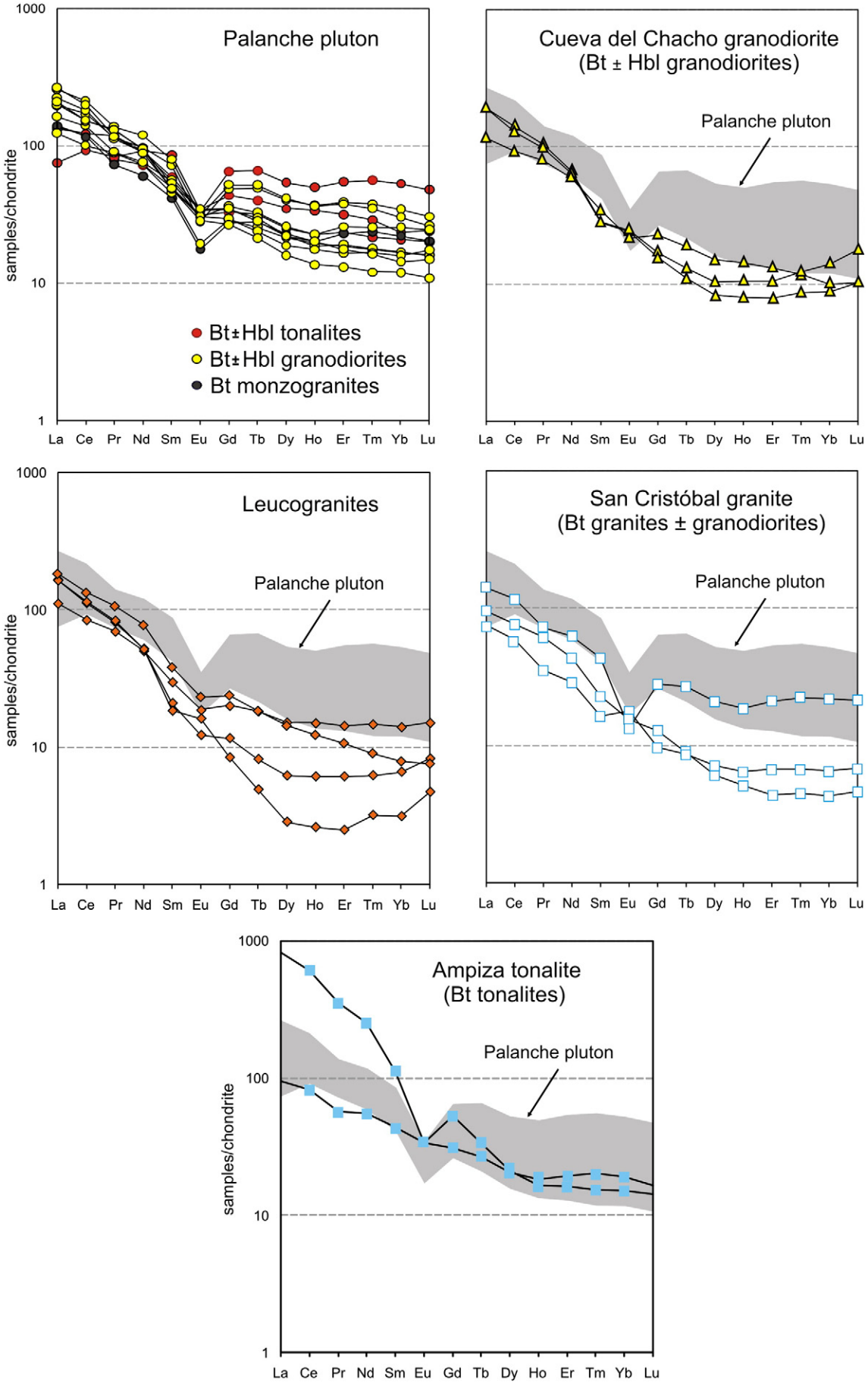
Palanche pluton
Bt±Hbl tonalites
Bt±Hbl granodiorites
Bt monzogranites
Cueva del Chacho granodiorite
(Bt ± Hbl granodiorites)
Palanche pluton
Leucogranites
Palanche pluton
San Cristóbal granite
(Bt granites ± granodiorites)
Palanche pluton
Ampiza tonalite
(Bt tonalites)
Palanche pluton
samples/chondrite
1000
100
10
1
La Ce Pr Nd Sm Eu Gd Tb Dy Ho Er Tm Yb Lu

and amphibole clots indicate that mafic enclaves could correspond to basic magma pulses that entered into a partially crystallized magmatic chamber (Tobisch et al., 1997).

Large mafic bodies (>100 m) are not found in the Palanche pluton, in contrast with other areas of the I-type Lower Ordovician granitic belt, such as the western part of the Sierra de Famatina (e.g., Aceñolaza et al., 1996) and the Sierra de Valle Fértil (e.g., Baldo et al., 1999; Otamendi et al., 2009a,b; Castro et al., 2014). Dismembered mafic bodies with sizes up to 10 m are present in some parts of Palanche pluton (Fig. 5b, c). Sometimes they show mingling with the host granitoid, generating rocks with different degrees of hybridization (Fig. 5d, e). The hybrid rocks are gray granodiorites to dark diorites, fine- to medium grained and inequigranular. The mineral association is Qtz + Pl + Mc + Bt (eastonite mainly) + Ttn + Ap + Zrn ± Amp (magnesio-hornblende and tschermakite). Amphibole clots and coronitic quartz are often present indicating a mechanical interaction between a partially crystallized granitic magma and basic magma (Zorpi et al., 1989; Castro et al., 1990; Hibbard, 1991). Finally, dark-gray, fine-grained, equigranular mafic rocks are also present occasionally as late dykes showing sharp contacts with the host granitic rocks. The presence of these mafic dykes may be associated with pegmatite veins.

6. Whole rock chemistry

A total of 18 samples were analyzed for major and trace elements. Of these 12 correspond to the Palanche pluton (including 4 samples of leucogranites), 4 to the Cueva de Chacho granodiorite and 2 are enclaves in the Palanche pluton, one of these is mafic and the other is tonalitic. Analyses of these samples are listed in Table 2 and their location is given in the map of Fig. 2b. In addition,10 samples of Palanche pluton, 2 mafic enclaves, 2 samples of the Cueva del Chacho Granodiorite, 2 of the Ampiza Tonalite and 7 of the San Cristóbal granite after data by Bellos (2005), Bellos et al. (2010) and Grosse et al. (2011) are projected in the diagrams.

6.1. Major elements

According to the Frost et al.'s (2001) classification scheme, the intrusive units are of magnesian-type (Fig. 3a) and evolve close to the boundary separating calcic and calc-alkalic series according to Peacock's alkali-lime index (Fig. 3b). The Palanche pluton is composed of mostly metaluminous (alumina saturation index: ASI < 1) tonalites, granodiorites and less abundant monzogranites. The other units and the leucogranites have moderate peraluminosity (1 < ASI < 1.2; Table 2). They plot very close to typical Cordilleran granitoid batholiths (Fig. 3).

The granitoids of the Palanche pluton (including the leucogranites) show a wide compositional range (≈60–75 wt.% SiO2) and an ASI index varying from 0.81 to 1.13. In the Harker diagrams (Fig. 6) all the analyzed rocks, but particularly those of the Palanche pluton, show a linear continuous trend. A negative correlation is found against silica for oxides FeO, MgO, Al_2O_3, TiO_2 and CaO. With respect to alkalis, K_2O has a positive correlation, although with greater dispersion than the rest of the oxides, whereas Na_2O shows a nearly flat pattern. These trends are indicative of a general evolution in relation to magmatic differentiation. The Harker trends are almost coincident with data from the typical Cordilleran Peninsular Range batholith (Fig. 6), with only appreciable differences in the alkalis: the Velasco rocks, with the exception of the two samples of the Ampiza tonalite, are clearly richer in K_2O and poorer in Na_2O compared with this Cordilleran batholith.

6.2. Trace elements

Regarding trace elements, samples of the SVB are characterized by low Sr contents (90–250 ppm) and low Sr/Y ratios (Sr/Y < 12, only one sample has Sr/Y > 12). In general, all samples of the calc-alkaline series of the SVB show the typical depletion in Nb and Ti and enrichment in Ba, Rb, Th and K, characteristic of arc settings (Fig. 7). A distinctive feature of the Velasco rocks is the depletion in Sr and P (Fig. 7) in comparison with typical continental arc andesites (red line in Fig. 7, after averaged values given by Kelemen et al. (2003)). Also interesting to note is the position of the Velasco rocks in the Nb–Y and Ta–Yb diagrams (Pearce et al., 1984, Fig. 8). With respect to Ta–Yb, they plot outside the field of VAG (Volcanic Arc Granites), because relative enrichment in Ta.

Chondrite-normalized (Sun and McDonough, 1989) REE plots are shown in Fig. 9. The Palanche pluton shows negative Eu anomaly (Eu/Eu^* ~ 0.45–1.30, average = 0.63), compatible with feldspar fractionation, and La_N/Yb_N ratios (N denoting chondrite-normalized values) in the range of 1.50–23.30 (average 9.19). The leucogranites have negative Eu anomaly (Eu/Eu^* average = 0.78), and a strong fractionation of REE (La_N/Yb_N average = 19.77) with exception of one of them, which has positive anomaly and a higher LREE/HREE fractionation. The patterns for LREE are similar to the other granitoids, but are more depleted in HREE. Samples of the Ampiza tonalite have variable negative Eu anomalies (Eu/Eu^* = 0.44–0.92) and a strong fractionation of the LREE in one of the samples. The Cueva del Chacho granodiorites have both positive and negative Eu anomaly (Eu/Eu^* = 0.77–1.16) and La_N/Yb_N = 12.24–23.24. Two samples of San Cristóbal granite show negative Eu anomaly (Eu/Eu^* = 0.38–0.91) and another one shows positive Eu anomaly (Eu/Eu^* = 1.42). The three samples show similar patterns of LREE but one of them shows a low LREE/HREE fractionation (La_N/Yb_N = 6.83). In general, the San Cristóbal granite is more depleted in REE than the Palanche pluton, but the patterns are very similar with gentle slopes for the LREE, and flat patterns of the HREE.

7. SHRIMP zircon ages

7.1. U–Th–Pb geochronology results

Eight samples were selected for the geochronological study. Morphological features of zircons in all samples are very similar, and we can group them in two types: simple prismatic crystals with concentric oscillatory zoning and simple elongated zircons with parallel-banded zonation, being the first type more abundant. U–Pb ages show a long-lived process of 45 Ma for the batholith building, ranging from 485 to 440 Ma. Older ages (500–520 Ma) are found, possibly related to Pampean orogeny (Drobe et al., 2009; Martino et al., 2009). Location of samples is given in Fig. 2b. Analytical results are listed in Table 3. Concordia diagrams and representative zircon crystals from each sample are shown in Fig. 10.

Of all samples for geochronology, six were collected in an area of the Palanche pluton at the Quebrada del Manzano (Fig. 2b). The area shows complex relations between granitic facies of the pluton and heterogeneous mafic rocks. These field relations were described above. Geochronologic relations are shown here.

7.1.1. Sample 8072: western flank (29° 47′43,7″–67° 08′ 00,5″)

It is a Hbl–Bt tonalite, the dominant assemblage is Qtz + Pl + Hbl + Bt + Mc + Ttn + opaque. Zircon and apatite are accessory minerals. Plagioclase ($An_{26–34}$, 65 vol.%) forms subhedral to anhedral (2–4 mm length), sometimes slightly zoned crystals. It is altered to sericite, kaolinite, calcite and epidote (pistacite and less clinozoisite). Quartz (18 vol.%) is anhedral and interstitial. Hornblende (14 vol.%, #Mg = 0.54–0.67) occurs as subhedral to anhedral crystals with small inclusions of opaque minerals. Biotite (2 vol.%, #Mg = 0.52–0.53) is subhedral with irregular edges. It is sometimes associated with hornblende and altered to chlorite. Mafic minerals have a size of up to 2 mm. Small titanite crystals (<1 vol.%) are present associated to hornblende. Zircons from this sample are simple, euhedral and large crystals (100–250 μm). They mostly show concentric zonation and inherited cores are not identifiable. The concordant group of ages

Table 3
SHRIMP U–Pb–Th analytical data of zircons.

Spot	f206	ppm U	ppm Th	Th/U	ppm ^{206}Pb[a]	$^{207}Pb^*/^{206}Pb^*$	± %	$^{206}Pb^*/^{238}U$	± %	$^{207}Pb^*/^{235}U$	± %	$^{207}Pb/^{206}Pb$ age	±	$^{206}Pb/^{238}U$ age	±	% disk.
8072: Tonalite																
1.1	0.69	372	416	1.15	22	0.0586	4.9	0.0681	1.5	0.550	5.1	551	110	425	6	23
2.1	0.41	373	51	0.14	22	0.0600	2.1	0.0676	1.3	0.560	2.4	605	45	422	5.1	30
3.1	1.02	373	45	0.12	23	0.0870	6.7	0.0703	1.5	0.843	6.9	1360	130	438	6.3	68
4.1	0.72	264	188	0.74	16	0.0621	4.1	0.0718	1.3	0.615	4.3	676	88	447	5.6	34
5.1	0.85	239	150	0.65	16	0.0592	3.5	0.0761	1.4	0.621	3.8	575	77	473	6.3	18
6.1	0.11	502	682	1.40	33	0.0581	1.3	0.0754	1.2	0.604	1.8	532	28	469	5.6	12
7.1	0.43	576	638	1.14	38	0.0562	2.3	0.0754	1.2	0.585	2.6	462	50	469	5.5	−1
8.1	1.87	252	316	1.30	16	0.0587	7.7	0.0735	1.4	0.594	7.8	554	170	457	6.3	18
8075: Granite																
1.1	0.37	398	318	0.82	26	0.0570	1.1	0.0764	0.9	0.600	1.5	490	24	475	4.1	0.6
3.1	0.59	243	43	0.18	16	0.0592	0.7	0.0777	0.7	0.635	1.1	576	16	482	3.1	3.4
4.1	0.38	228	259	1.17	15	0.0589	0.9	0.0763	1.5	0.620	1.8	564	20	474	6.8	3.2
5.1	0.12	370	253	0.70	24	0.0586	0.7	0.0765	0.5	0.618	0.9	552	16	475	2.3	2.8
6.1	0.33	228	109	0.49	15	0.0586	1.0	0.0772	0.8	0.624	1.3	554	22	479	3.6	2.6
6.2	0.68	402	190	0.48	27	0.0578	1.6	0.0772	0.4	0.615	1.7	521	35	480	1.7	1.4
7.1	0.08	485	146	0.31	33	0.0591	1.9	0.0772	1.0	0.629	2.1	572	41	479	4.4	3.2
8.1	0.41	718	516	0.74	47	0.0586	1.2	0.0760	0.6	0.613	1.4	552	25	472	2.9	2.8
9.1	0.56	156	196	1.29	11	0.0603	2.1	0.0781	1.3	0.649	2.5	614	46	485	6	4.6
10.1	0.49	967	848	0.90	63	0.0600	0.3	0.0751	0.3	0.621	0.5	603	6	467	1.4	4.8
13.2	1.06	479	143	0.31	31	0.0593	0.8	0.0758	0.5	0.620	1.0	578	17	471	2.4	3.8
15.1	0.24	767	608	0.81	51	0.0586	0.6	0.0765	1.1	0.619	1.3	553	13	476	5.1	2.8
16.1	0.37	549	521	0.97	36	0.0581	1.0	0.0756	0.7	0.605	1.3	532	22	470	3.1	2.2
17.1	0.59	260	317	1.25	17	0.0588	0.2	0.0754	0.3	0.611	0.5	560	4	469	1.5	3.2
18.1	0.67	299	297	1.02	19	0.0590	0.4	0.0752	0.5	0.612	0.7	568	8	468	2.3	3.6
19.1	0.33	319	523	1.68	20	0.0593	0.8	0.0759	1.3	0.621	1.5	578	18	472	5.7	3.8
22.1	0.19	758	467	0.63	50	0.0584	0.9	0.0762	0.4	0.613	1.1	545	20	473	2	2.6
8076: Monzogranite																
1.1	0.88	330	203	0.64	22	0.0545	4.5	0.0755	1.3	0.568	4.7	393	100	469	6	−19
2.1	0.49	585	317	0.56	38	0.0559	1.9	0.0760	1.2	0.586	2.3	449	42	472	5.5	−5
3.1	0.70	403	229	0.59	27	0.0557	2.8	0.0759	1.3	0.583	3.1	442	63	472	5.7	−7
4.1	1.49	228	136	0.62	15	0.0539	8.3	0.0726	1.4	0.539	8.4	367	190	452	6.2	−23
5.1	1.36	306	481	1.63	20	0.0555	6	0.0767	1.3	0.588	6.2	434	130	477	6.1	−10
6.1	0.81	462	630	1.41	31	0.0555	3.3	0.0782	1.5	0.599	3.6	434	74	485	6.8	−12
7.1	0.31	784	717	0.95	57	0.0572	1.4	0.0844	1.3	0.665	1.9	499	30	522	6.4	−5
8077: Tonalite																
1.1	0.69	290	241	0.85	19	0.0577	0.8	0.0751	0.7	0.598	1.2	520	19	467	3.3	1.8
1.2	0.42	260	186	0.73	17	0.0571	0.3	0.0763	0.4	0.601	0.6	496	7	474	1.6	0.8
2.1	0.36	481	455	0.97	32	0.0564	0.9	0.0759	0.4	0.590	1.0	468	20	472	1.9	−0.2
3.1	0.28	567	453	0.82	36	0.0575	1.0	0.0741	1.1	0.587	1.5	511	21	461	4.7	1.8
4.1	0.11	490	293	0.61	32	0.0574	1.5	0.0744	2.2	0.589	2.7	508	34	462	9.7	1.6
5.2	0.58	319	287	0.92	21	0.0583	1.9	0.0768	0.8	0.618	2.1	542	42	477	3.9	2.4
6.1	0.26	246	153	0.64	16	0.0577	1.4	0.0749	1.6	0.596	2.1	517	30	466	7.2	1.8
8.1	0.97	271	202	0.77	18	0.0600	1.0	0.0765	0.8	0.633	1.3	604	21	475	3.7	4.6
9.1	0.10	175	266	1.56	11	0.0591	0.2	0.0751	0.8	0.611	0.9	570	5	467	3.7	3.6
9.2	−0.13	157	58	0.38	10	0.0592	0.9	0.0748	0.8	0.611	1.2	576	19	465	3.7	4
10.1	0.43	384	452	1.21	25	0.0584	1.0	0.0742	1.7	0.598	2.0	546	22	461	7.5	3
11.1	0.26	428	330	0.79	28	0.0574	1.1	0.0768	0.4	0.607	1.2	505	24	477	1.9	1
11.2	0.11	897	606	0.69	58	0.0579	0.6	0.0750	0.4	0.598	0.8	525	12	466	1.6	2
12.1	0.58	532	890	1.72	35	0.0591	0.3	0.0756	0.8	0.616	0.9	570	5	470	3.4	3.6
13.1	0.29	276	327	1.22	18	0.0580	1.3	0.0759	1.4	0.607	1.9	531	29	471	6.3	2.2
14.2	0.33	930	1017	1.12	59	0.0593	0.7	0.0736	0.6	0.602	1.0	578	15	458	2.7	4.2
15.2	0.50	266	39	0.15	17	0.0592	1.9	0.0750	0.7	0.612	2.0	574	41	466	3	3.8
16.1	0.13	1140	880	0.79	75	0.0575	0.7	0.0758	0.7	0.601	1.1	510	16	471	3.2	1.4
17.1	0.16	1191	238	0.2	79	0.0569	0.5	0.0771	0.7	0.605	0.9	487	10	479	3.4	0.2
18.1	0.42	448	395	0.9	29	0.0565	0.9	0.0749	0.8	0.583	1.3	471	21	466	3.6	0.2
18.2	0.19	378	292	0.79	25	0.0578	0.7	0.0759	1.2	0.605	1.4	521	15	472	5.5	1.8
19.1	0.20	335	91	0.28	22	0.0571	1.6	0.0754	1.1	0.594	2.0	494	36	469	5	1
20.1	0.39	560	515	0.94	36	0.0578	0.7	0.0743	0.9	0.592	1.2	522	15	462	4.1	2.2
21.1	0.31	490	159	0.33	32	0.0567	0.9	0.0758	0.8	0.593	1.2	481	20	471	3.5	0.4
21.2	0.21	1030	228	0.23	66	0.0575	0.4	0.0737	1.3	0.584	1.4	510	9	458	5.7	1.8
23.1	0.29	752	564	0.77	49	0.0564	0.5	0.0756	0.7	0.588	0.9	469	10	470	3.1	0
24.1	0.17	679	406	0.61	45	0.0568	0.7	0.0767	0.3	0.600	0.8	482	15	477	1.4	0.2
25.2	1.52	180	67	0.38	12	0.0576	1.6	0.0757	1.3	0.601	2.1	514	36	470	6.1	1.6
26.1	0.76	262	153	0.6	17	0.0588	1.3	0.0762	1.0	0.617	1.6	558	28	473	4.4	3
26.3	0.33	328	191	0.6	21	0.0580	0.4	0.0734	0.4	0.587	0.7	530	9	457	2	2.6
8078: Granodiorite																
1.1	0.96	283	189	0.69	17	0.0614	5.3	0.0696	3	0.589	6.1	652	110	434	13	33
2.1	1.36	350	294	0.87	22	0.0567	7.7	0.0710	1.6	0.556	7.9	482	170	442	6.7	8
3.1	1.65	402	529	1.36	25	0.0553	7.3	0.0715	1.3	0.545	7.4	425	160	445	5.5	−5
4.1	3.07	152	80	0.54	9	0.0587	9.7	0.0700	1.5	0.567	9.8	556	210	436	6.3	21
5.1	0.66	524	531	1.05	32	0.0567	2.6	0.0710	1.2	0.555	2.9	480	57	442	5.2	8

(continued on next page)

Table 3 (*continued*)

Spot	f206	ppm U	ppm Th	Th/U	ppm ^{206}Pb[a]	$^{207}Pb^*/^{206}Pb^*$	± %	$^{206}Pb^*/^{238}U$	± %	$^{207}Pb^*/^{235}U$	± %	$^{207}Pb/^{206}Pb$ age	±	$^{206}Pb/^{238}U$ age	±	% disk.
8078: Granodiorite																
6.1	2.02	253	284	1.16	16	0.0564	7.4	0.0711	1.3	0.553	7.5	467	160	443	5.8	5
7.1	0.88	402	260	0.67	25	0.0606	2.8	0.0709	1.3	0.593	3	626	60	442	5.4	29
8079: Monzogranite																
1.1	1.21	198	182	0.95	13	0.0564	4.9	0.0745	0.8	0.580	5	467	110	464	3.6	1
2.1	0.62	207	118	0.59	14	0.0587	2.9	0.0775	1.1	0.627	3.1	556	63	481	5	13
3.1	0.96	346	58	0.17	23	0.0555	3.3	0.0755	0.6	0.577	3.4	431	74	469	2.7	−9
4.1	0.62	412	180	0.45	27	0.0558	2.7	0.0762	0.6	0.586	2.8	445	60	473	2.8	−6
5.1	1.09	351	97	0.29	23	0.0546	3.9	0.0764	0.6	0.575	3.9	395	86	475	2.7	−20
6.1	1.18	381	49	0.13	25	0.0564	7	0.0758	0.7	0.589	7.1	467	160	471	3.2	−1
8080: Hybrid mafic rock																
1.1	0.81	404	60	0.15	26	0.0561	2.5	0.0728	2.2	0.563	3.3	455	57	453	9.5	1
1.2	0.17	412	295	0.74	26	0.0562	1.5	0.0724	2.1	0.561	2.6	461	34	451	9.3	2
2.1	0.16	362	72	0.21	24	0.0553	1.5	0.0759	2.2	0.578	2.6	424	33	471	9.8	−11
3.1	0.54	137	107	0.81	9	0.0543	3.6	0.0731	2.3	0.547	4.3	383	82	455	10	−19
4.1	0.10	424	48	0.12	30	0.0569	1.3	0.0817	2.2	0.641	2.6	487	29	506	11	−4
5.1	0.58	234	272	1.20	15	0.0532	3.1	0.0745	2.2	0.546	3.8	336	69	463	9.8	−38
6.1	0.71	282	44	0.16	20	0.0567	3	0.0834	2.2	0.652	3.7	480	67	516	11	−8
7.1	0.09	673	528	0.81	48	0.0564	1.1	0.0832	2.1	0.647	2.4	467	25	515	11	−10
8.1	0.53	304	139	0.47	19	0.0547	3.2	0.0735	2.4	0.555	4	401	71	457	11	−14
9.1	0.14	883	586	0.69	55	0.0558	1.1	0.0724	2.1	0.556	2.4	442	24	451	9.2	−2
8081: Granite																
1.1	0.13	721	120	0.17	47	0.0553	1.1	0.0750	2.1	0.572	2.4	426	24	466	9.6	−9
2.1	0.23	345	250	0.75	22	0.0542	1.9	0.0742	2.2	0.554	2.9	378	44	461	9.6	−22
3.1	0.42	217	146	0.70	14	0.0560	2.3	0.0756	2.2	0.583	3.2	452	51	470	10	−4
4.1	0.47	277	254	0.95	18	0.0540	2.6	0.0740	2.3	0.551	3.5	372	58	460	10	−24
5.1	0.41	251	175	0.72	17	0.0536	2.4	0.0766	2.2	0.566	3.2	354	54	476	10	−34
6.1	0.27	429	332	0.80	28	0.0564	1.6	0.0761	2.4	0.591	2.9	466	35	473	11	−1
7.1	0.25	228	220	1.00	17	0.0569	2.5	0.0842	2.2	0.661	3.3	489	54	521	11	−7
8.1	0.81	176	151	0.89	11	0.0539	4.4	0.0744	2.2	0.553	4.9	366	99	463	10	−26

f206 = (common ^{206}Pb) / (total measured ^{206}Pb) based on measured ^{204}Pb.
Pb* indicates the radiogenic portion.
Samples 8075 and 8077: errors are at 95% confidence interval.
Samples 8072, 8076, 8078 to 8081: errors are 1-sigma.
[a] Common Pb corrected using measured ^{204}Pb.

(4 analyses) give $^{206}Pb/^{238}U$ ages between 473 ± 6.3 and 457 ± 6.3 Ma, yielding a concordia age of 468 ± 8.5 Ma (MSWD = 1.5). Other 4 analyses show younger ages (between 447 ± 5.6 and 422 ± 5.1 Ma) and high discordance percentages (>20%).

7.1.2. Sample 8075: Quebrada del Manzano (29° 42′ 46″–67° 07′ 56,3″)

This sample is a coarse grained granite composed of Qtz + Pl + Kfs + Bt + Ep and Mag, Mn-Ilm, Ttn and Zrn as main accessory phases. Plagioclase ($An_{47–43}$) appears as subhedral grains with quartz and K-feldspar, with albite rims in contacts. Biotite (#Mg = 0.38–0.40) is present in clots with accessory phases or as subhedral individual grains with quartz, plagioclase and K-feldspar. Epidote, magnetite and Mn-ilmenite appear often grouped as inclusions in main phases and biotite clots. Selected zircons from this sample are mainly medium–large euhedral crystals (80–180 μm) with concentric oscillatory zoning. Inner and external areas of zircons have been analyzed (17 spots) yielding $^{206}Pb/^{238}U$ ages between 485 ± 6 and 467 ± 1.4 Ma and a concordia age of 472 ± 2.9 Ma (MSWD = 0.74).

7.1.3. Sample 8076: Quebrada del Manzano (29° 42′46″–67° 07′ 56,3″)

This sample is a medium-grained monzogranite. It is composed of Qtz + Pl + Mc + Bt + Ttn + Aln. Quartz (37 vol.%) forms anhedral and very irregular crystals of up to 3.5 mm. Plagioclase ($An_{29–37}$, 21 vol.%) is anhedral to subhedral and sometimes it is partially included in quartz or microcline. Plagioclase is slightly zoned and its size is of up to 3.5 mm. Microcline (39 vol.%) forms anhedral crystals of up to 5 mm length and may contain inclusions of plagioclase, biotite and quartz. Biotite is very scarce (2 vol.%, #Mg = 0.42–0.52) forming anhedral crystals sometimes chloritized and with inclusions of rutile needles. Titanite and allanite, opaques, zircon and apatite are accessory minerals, mostly included in biotite. This sample contains simple, euhedral zircons. They are large crystals (150–300 μm) with concentric or parallel-banded zoning. A main group of analyses (5 analyses) gives $^{206}Pb/^{238}U$ ages between 485 ± 6.8 and 469 ± 6 Ma and yields a concordia age of 474 ± 5.4 Ma (MSWD = 0.6). A simple parallel-banded zircon gives an older age (522 ± 6.4 Ma) and the external area of a simple crystal yields the youngest age (452 ± 6.2 Ma).

7.1.4. Sample 8077: Quebrada del Manzano (29° 42′ 46″–67° 07′ 56,3″)

This sample is a mafic tonalitic enclave in the sample 8076 and is composed of Pl + Qtz + Bt + Hbl + Kfs + Ttn, with Mag, Ap and Zrn as main accessory minerals. Plagioclase ($An_{59–53}$) appears as subhedral to anhedral grains associated with quartz and microcline or as large zoned crystals with a rim of secondary minerals, and inclusions of biotite and hornblende. It has been altered to sericite, kaolinite, calcite, pistacite and clinozoisite. Quartz forms abundant and irregular grains of minor size than plagioclase. Microcline is scarce and interstitial and sometimes is perthitic or presents myrmekites in their contacts. Biotite (#Mg =0.51–0.48) is more abundant than hornblende and is present as subhedral grains, sometimes chloritized. Hornblende crystals (#Mg = 0.52–0.48) appear grouped in clots with magnetite and titanite; the latter also forms interstitial crystals between plagioclase. Selected zircon crystals are medium–large (100–250 μm), simple and euhedral crystals. They mostly show concentric oscillatory zoning, where several growing phases are distinguishable. Some of these zircon rims yield ages that differ various million years from those of inner areas (i.e. zircons 1, 11 and 21, Table 3). Thirty concordant analyses give $^{206}Pb/^{238}U$ ages between 479 ± 3.4 and 457 ± 2 Ma and yield a concordia age of 470 ± 2.5 Ma (MSWD = 0.92).

7.1.5. Sample 8078: Quebrada del Manzano (29° 42′46″–67° 07′ 56,3″)

This sample is a medium-grained Bt-Hbl granodiorite. It is composed of Qtz + Pl + Mc + Bt + Hbl + Ttn. Plagioclase ($An_{36–40}$, 33 vol.%) is anhedral and its crystallization is later than that of hornblende (edenite and ferro-edenite), biotite and titanite, and occupies spaces between these minerals. Microcline (15 vol.%) forms anhedral crystals of size very variable from interstitial to large crystals (up to 5 mm). Sometimes it is perthitic and may have myrmekites around the edges. Quartz (34 vol.%) forms anhedral and very irregular crystals. Biotite (15 vol.%, #Mg = 0.50–0.56) is present as anhedral to subhedral crystals, whereas hornblende (3 vol.%, #Mg = 0.47–0.57) is anhedral and usually associated with biotite. Titanite, opaques, zircon and apatite are accessory minerals. Zircons from this sample are mainly simple, elongated and parallel banded crystals, with a lower proportion of concentric zoned zircons. Ages are between 445 ± 5.5 and 436 ± 6.3 Ma and give a concordia age of 442 ± 5.1 Ma (N = 6, MSWD = 0.5).

7.1.6. Sample 8079: Quebrada del Manzano (29° 42′46″–67° 07′ 56,3″)

This sample is a Bt–Hbl monzogranite. It is composed of Qtz + Pl + Mc + Bt + Hbl + Ttn. Plagioclase (An_{41}, 41 vol.%) is anhedral to subhedral and slightly zoned. Microcline (27 vol.%) forms anhedral crystals of up to 5 mm, sometimes it is perthitic and may show myrmekites around the edges. It contains inclusions of plagioclase, biotite and quartz. Quartz (18 vol.%) forms anhedral and very irregular crystals. Biotite (12 vol.%, #Mg = 0.33–0.42) is present as anhedral to subhedral crystals whereas hornblende (1 vol.%, #Mg = 0.52–0.53) is anhedral and usually associated with biotite. Prismatic allanite, titanite, opaques, zircon and apatite are accessory minerals. Zircons from this sample are mostly euhedral, simple crystals with concentric oscillatory zoning. Discontinuous cores or recrystallization areas are scarce. Six analyses give $^{206}Pb/^{238}U$ ages between 481 ± 5 and 464 ± 3.6 Ma, yielding a concordia age of 472 ± 3.2 Ma (MSWD = 1.3).

7.1.7. Sample 8080: Quebrada del Manzano (29° 42′46″–67° 07′ 56,3″)

This is a hybrid mafic rock formed by abundant crystals of plagioclase ($An_{43–46}$), biotite and hornblende, quartz as little grains or large xenocrysts and scarce potassic feldspar. Two different sizes of plagioclase crystals are present (38 vol.%). The biggest (3–5 mm) is subhedral and zoned, some of them have a ring of inclusions and alteration minerals. They have abundant inclusions of biotite, hornblende and are very altered to pistacite, clinozoisite and sericite. Small and subhedral to anhedral crystals (0.25–1 mm) are also present in the rock. Quartz is abundant (43 vol.%) and forms anhedral little crystals or large xenocryst (up to 5 mm) surrounded by biotite, hornblende and less plagioclase. K-feldspar (4 vol.%) is present as poikilitic, perthitic and anhedral crystals that form a pavement between other minerals. Biotite (10 vol.%, #Mg = 0.49–0.53) and hornblende (1,5 vol.%, #Mg = 0.60–0.67) are associated. Anhedral to subhedral grains of titanite are present (3.5 vol.%). Zircon crystals from this sample are mainly simple, euhedral crystals with concentric or parallel banded zoning. A few crystal cores are distinguishable, however they show the same ages and continuity with the external areas of zircons. A main group of analyses gives $^{206}Pb/^{238}U$ ages between 457 ± 11 and 451 ± 9.2 Ma. We found older ages in this sample: three analyses give ages between 515 and 505 Ma, and

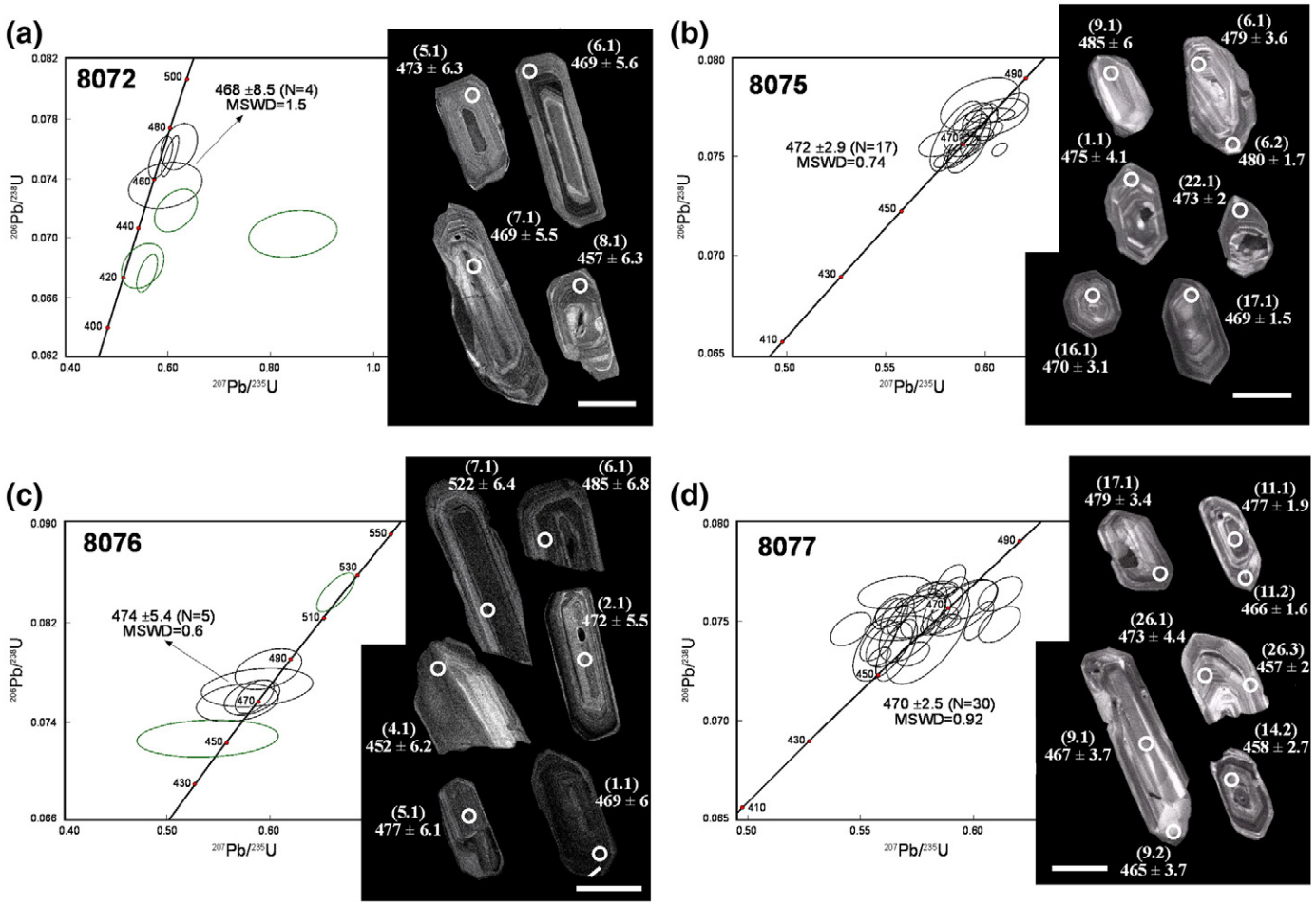

Fig. 10. Concordia U–Pb diagrams for the eight studied samples. Error ellipses for data points in the Concordia diagrams are 68.3% confidence limits, including the error from the standard. Light colored ovoids are analyses excluded to obtain the mean concordia ages. A representative selection of cathode luminiscence images of analyzed zircons in each sample is shown beside the concordia diagrams. Spots' location and their resulting $^{206}Pb/^{238}U$ ages (Ma) are indicated. Data are given in Table 3. Scale bars are 100 μm.

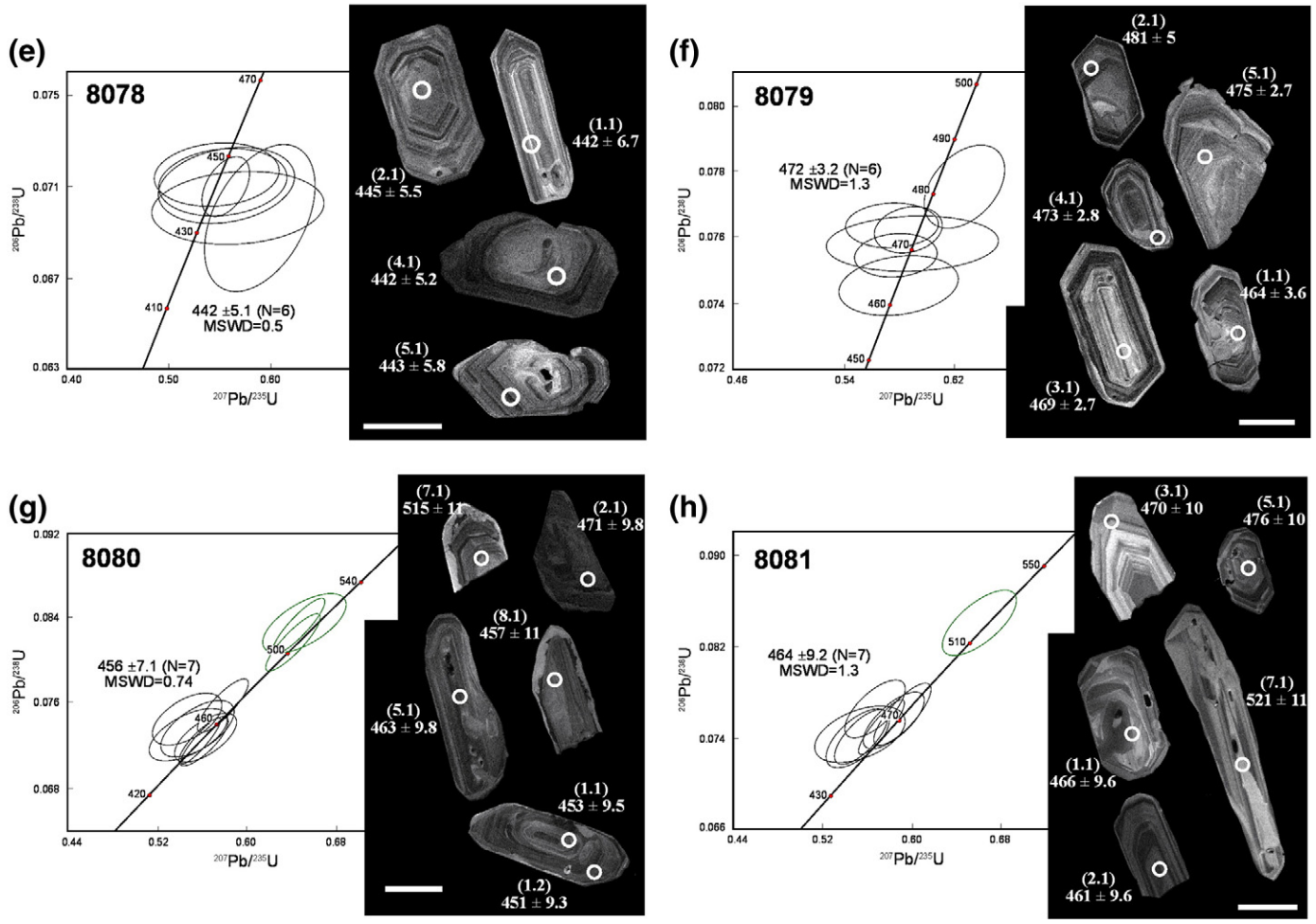

Fig. 10 (*continued*).

other two yield $^{206}Pb/^{238}U$ ages of 471 ± 9.8 Ma and 463 ± 9.8 Ma. Age variations have no relation with the morphological types or spot location. $^{206}Pb/^{238}U$ ages between 470 and 450 Ma yield a concordia age of 456 ± 7.1 Ma (N = 7, MSWD = 0.74).

7.1.8. Sample 8081: Cueva del Chacho (29° 58′ 26″–67° 04′ 59″)

This sample is a porphyritic Bt–Hbl granodiorite. The matrix is composed of Qtz + Pl + Bt + Hbl + Ttn. Microcline forms megacrysts of up to 3–4 cm but it is very scarce in the matrix (4 vol.%) and its size is of up to 6 mm. Myrmekites are present in the contact with plagioclase crystals. Plagioclase ($An_{38–47}$, 38 vol.%) is anhedral to subhedral and forms large crystals of up to 3 mm. Quartz (43 vol.%) forms anhedral and very irregular crystals of up to 4 mm. Biotite (10 vol.%, #Mg = 0.45–0.54) is present as subhedral crystals whereas hornblende (1.5 vol.%) is anhedral and associated with biotite. Titanite, opaques, zircon and apatite are accessory minerals mostly included in biotite. Selected zircons from this sample are large (150–300 μm), euhedral crystals with mostly concentric oscillatory zoning and few acicular parallel banded zircons. A main group of analyses gives $^{206}Pb/^{238}U$ ages between 460 ± 10 and 476 ± 10 Ma, yielding a concordia age of 464 ± 9.2 Ma (N = 7, MSWD = 1.3). A large, simple and parallel banded zircon gives an older age (522 ± 6.4 Ma).

8. Discussion

Age relations are reporting that part of the rocks forming the SVB corresponds to intrusion of magma pulses that were separated in time by several Ma (Fig. 11). Intrusive contacts and relations between granites and mafic rocks in the outcrops of Quebrada del Manzano are in agreement with age determinations and support a protracted process of multipulse injection and amalgamation in the construction of the batholith. However, gradual transitions between granitoid facies are also observed across the intrusive bodies, denoting that in-situ differentiation also was an operative process at the site of final emplacement. Criteria to distinguish multipulse from in-situ fractionation are discussed here through a combination of ages and geochemical relationships.

8.1. Deep pulses or in-situ fractionation

Evidence about the existence of protracted magma pulses in building-up the batholith is provided by field relations and contacts between intrusive rocks of the Quebrada del Manzano outcrops (Figs. 12 and 2b). Four samples of distinct facies yield very similar concordia ages ranging from 474 ± 5 to 470 ± 2 Ma, with differences within error. Furthermore, the patterns shown by the probability density distribution of U–Pb zircon ages (Fig. 11) are similar. These samples can be considered coeval, genetically linked and, thus, the fractionation process as produced in-situ, or at least produced at the time of emplacement in a possibly deeper magma reservoir. The significant number of analyses clustered between 470 and 474 Ma in these samples allows us to suggest that this age corresponds to a major event in the protracted building of the batholith, probably related to the main emplacement stage for the facies comprising Quebrada del Manzano.

However, many U–Pb SHRIMP ages yielded in most samples of Sierra de Velasco batholith are not within analytical error of mean calculated ages, implying that they represent different zircon crystallization ages,

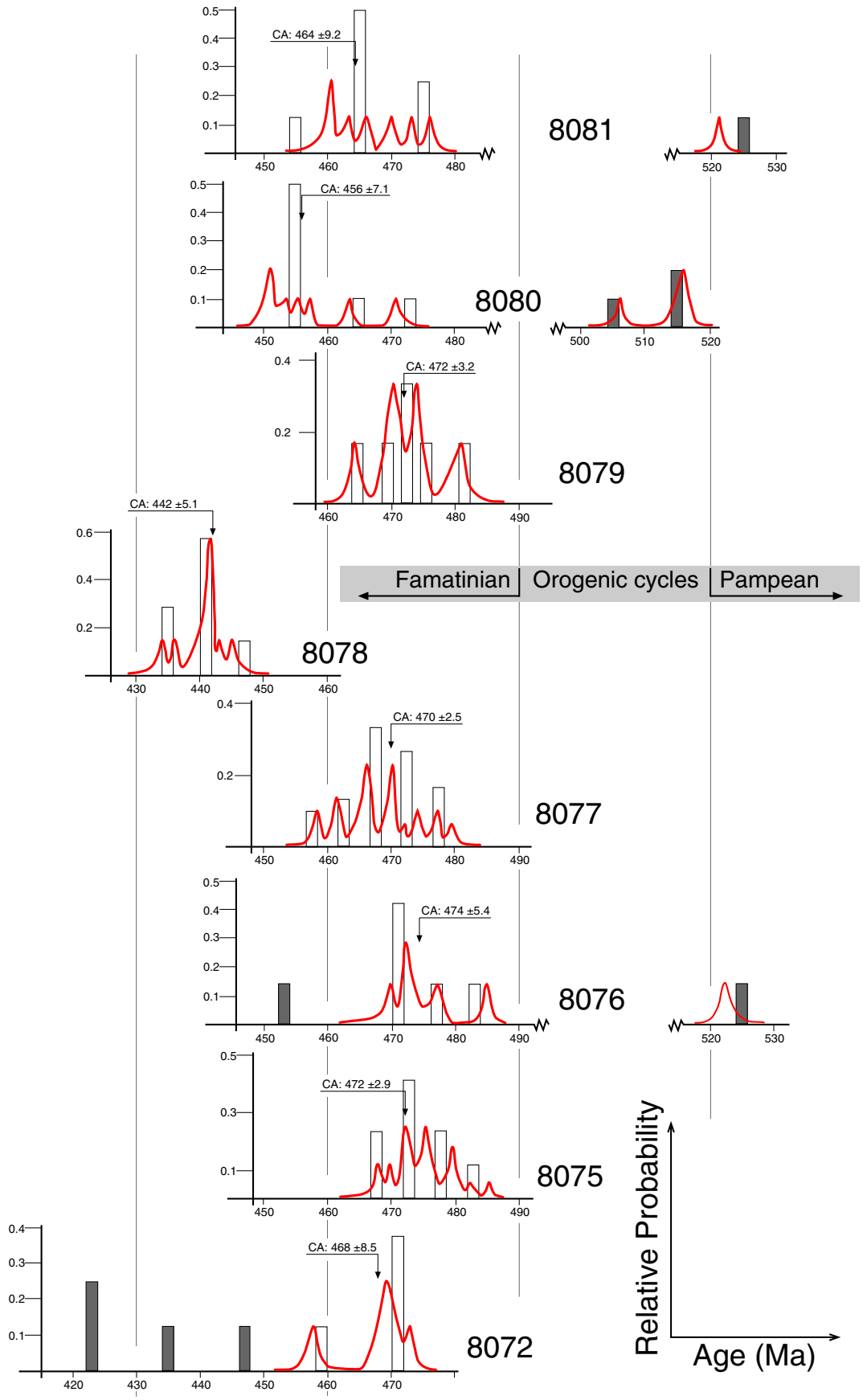

Fig. 11. Geochronological sketch of the Sierra de Velasco batholith. Figure is assembled with the relative probability histograms of each sample, which include the probability density distribution of U–Pb zircon ages (red lines). Gray bars are referred to ages not included in calculated concordia ages (high discordance analyses and inherited zircons). CA: concordia age.

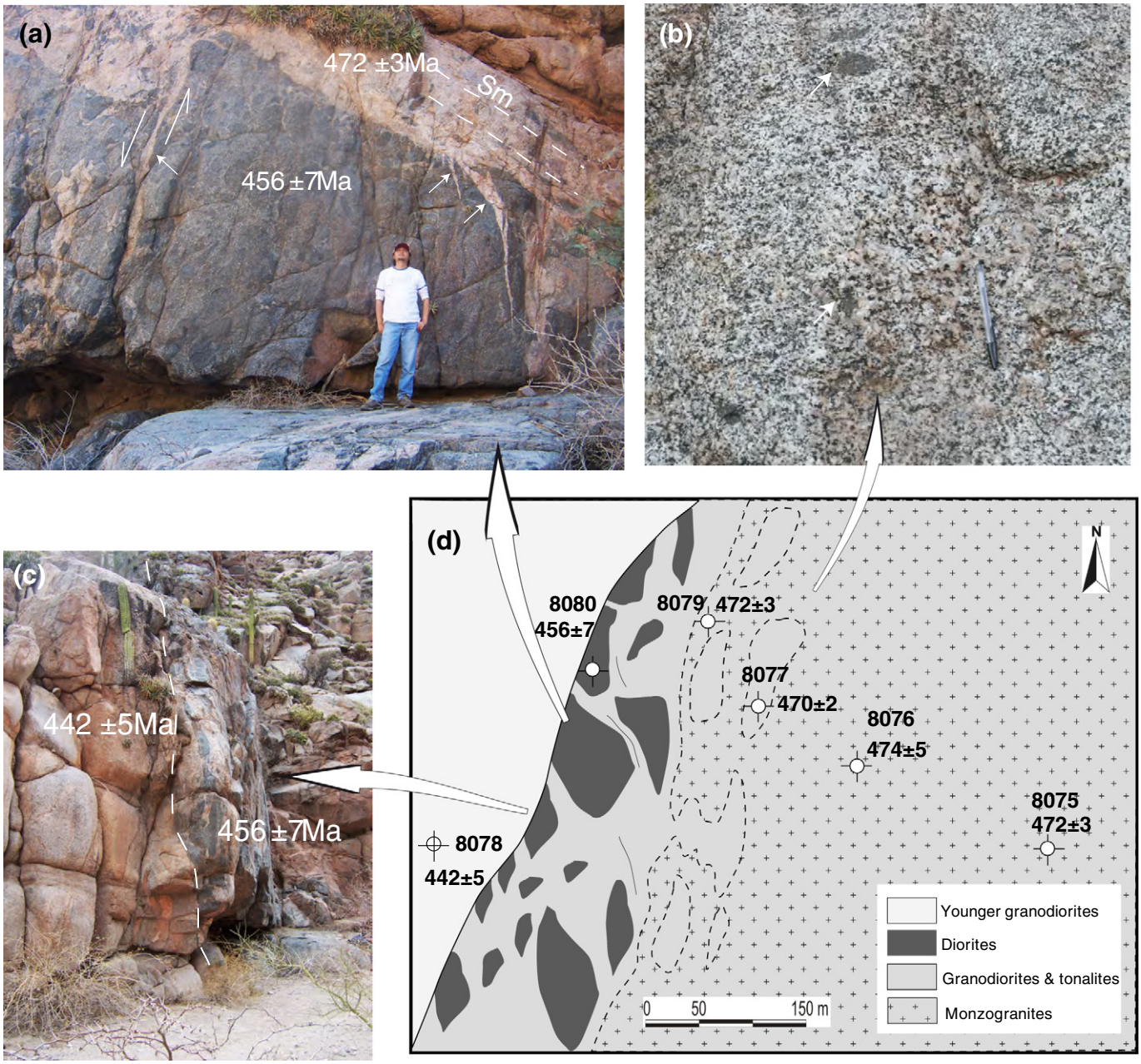

Fig. 12. Field relations between granite pulses and mafic rocks of the Palanche pluton at Quebrada del Manzano. (a) Details of the apparently synplutonic contact relationships between mafic bodies and host granodiorite showing magmatic shear zones and back veining at the contacts (white arrows) and magmatic foliation in the host. (b) Textural heterogeneities of the tonalite rocks showing abundant, cm-sized mafic enclaves and coarse-grained patches. (c) Sharp contact between a young pulse of granodiorite (442 Ma) cross-cutting the mafic bodies dated at 453 Ma. (d) Geological sketch of the Quebrada del Manzano outcrops showing intrusive relations and ages of magmatic pulses. See text for further details.

e.g., sample 8077, where zircon ages are between 479 ± 3 and 457 ± 2 Ma.

New insights in the knowledge of composite batholiths and sequential emplacement of magmas in the crust, combined with geochronological and thermo-numerical studies (e. g. Coleman et al., 2004; Miller et al., 2011; Paterson et al., 2011; Díaz-Alvarado et al., 2013), suggest the presence of high grade domains in the middle-lower crust over long periods of time, during the sequential emplacement and building of the large batholiths, and favoring the existence of large magma chambers composed of crystal mush and a significant liquid percentage. In the Sierra de Velasco batholith, the repeated occurrence of magmatic contacts between pulses and facies point out the existence of processes of continuous recharge and re-mobilization of melts, besides fractionation processes in the emplacement level. Thus, this results in the presence of

Fig. 13. Major-element plots showing cotectic and non-cotectic variations found in granitoids of the Sierra de Velasco batholith. (a) CaO–MgO diagram. (b) Pseudoternary projection onto the plane F (Fe + Mg + Mn)–An (Anorthite)–Or (Orthoclase). (c) Plot of the K# (= molar K_2O / (K_2O + CaO) against MgO. (d) Multicationic A–B diagram (Debon and Le Fort, 1983). In all diagrams, the red line represent the composition of cotectic liquids traced by extrapolation of experimental data on a water-bearing (2.5 wt.% water) andesite system (large blue star in (b)) at 300 MPa (Castro et al., 2013). Red dashed lines represent 20 and 40 mass% of assimilated pelite, calculated by mass balance from four separated points of the cotectic trend. See text for further details.

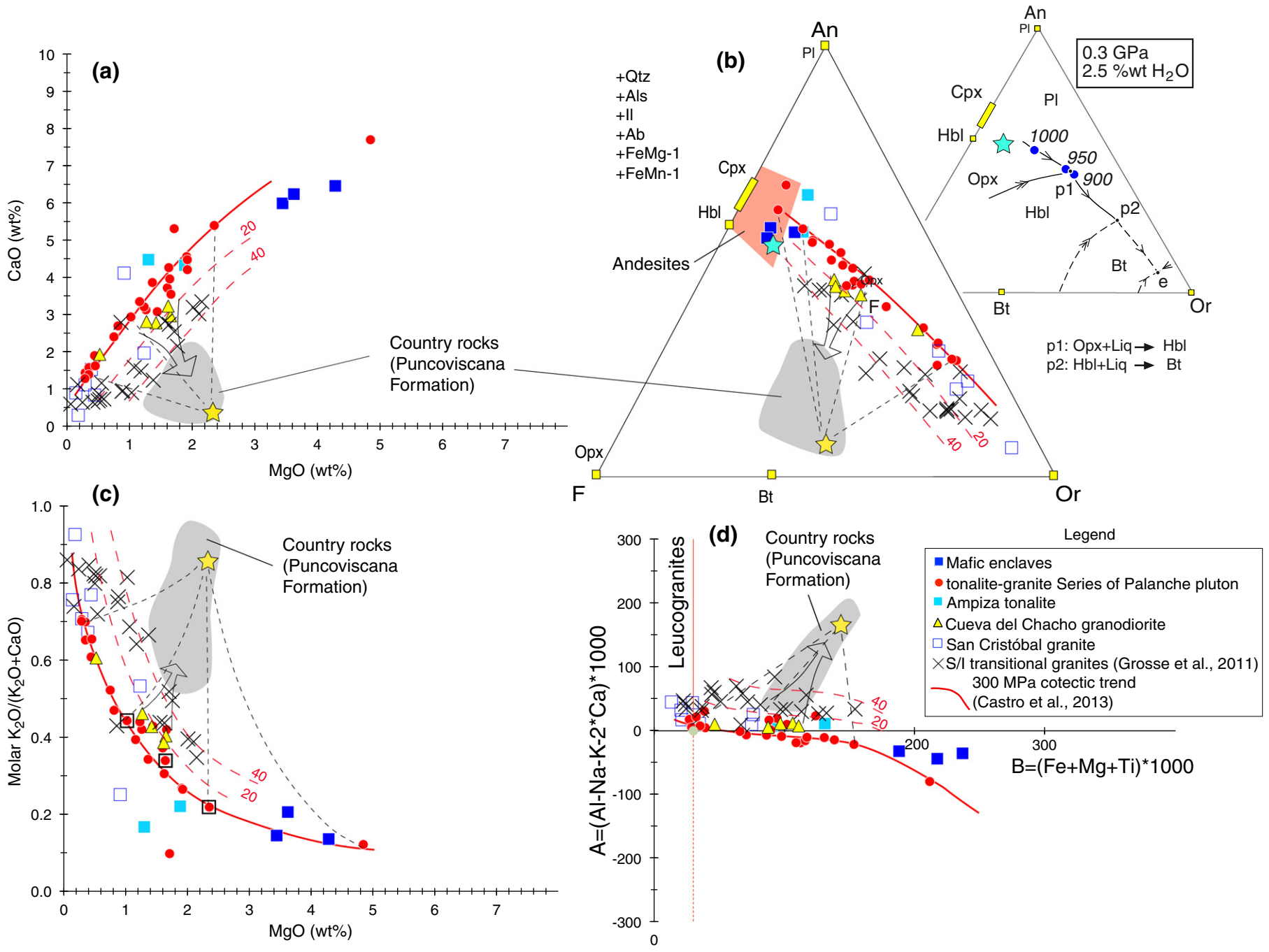
(a)
CaO (wt%)
MgO (wt%)
20
40
Country rocks
(Puncoviscana
Formation)
(b)
An
Pl
+Qtz
+Als
+Il
+Ab
+FeMg-1
+FeMn-1
Cpx
Hbl
Andesites
Opx
F
Bt
Or
0.3 GPa
2.5 %wt H2O
1000
950
900
p1
p2
e
p1: Opx+Liq → Hbl
p2: Hbl+Liq → Bt
(c)
Molar K2O/(K2O+CaO)
MgO (wt%)
Country rocks
(Puncoviscana
Formation)
(d)
Leucogranites
A=(Al-Na-K-2*Ca)*1000
B=(Fe+Mg+Ti)*1000
Country rocks
(Puncoviscana
Formation)
Legend
Mafic enclaves
tonalite-granite Series of Palanche pluton
Ampiza tonalite
Cueva del Chacho granodiorite
San Cristóbal granite
S/I transitional granites (Grosse et al., 2011)
300 MPa cotectic trend
(Castro et al., 2013)

ancient Famatinian zircons with other younger ones, or both ages in a single zircon (e.g., sample 8077: zircons 11 and 21), i.e., samples with more than 20 Ma ranges; pulses with younger ages (e.g., sample 8081) and the almost complete absence of solid-state deformation or intrusive contacts throughout the batholith. This interpretation requires that the distinct granitic sheets remained in a magmatic state for very long periods (>5 Ma), able to become rejuvenated by successive intrusions (Díaz-Alvarado et al., 2013).

Regarding the mafic rocks at the Quebrada del Manzano, field relations clearly indicate synplutonic intrusion of heterogeneous diorites into the host granodiorite. Among the field evidences is the presence of back-veining (see white arrows in Fig. 12a) clearly supporting the presence of a residual liquid in the host granodiorite and, thus, the magmatic nature of the host. Most of U–Pb ages obtained in the diorite sample (8080) are between 450 and 460 Ma, in agreement with the intrusive relations that they show in relation to the host granodiorite, which concordia age yields 472 ± 6 Ma, but containing zircons 15 Ma younger than those clustered around mean ages. This time difference of about 15 Ma between both magmatic systems would be in conflict with this interpretation whether the host granite was a solid rock, and not a magma, 15 Ma elapsed from magma emplacement to the arrival of the new mafic pulse. A possible explanation is that the mafic magma intruded into a granodiorite host composed by a crystal mush and a significant percentage of residual melt. The intrusion induced remobilization of remnant granitic melts and probably locally re-magmatization. These melts are back-veined into the partially crystallized intruding diorite. Melting of the host granodiorite is favored by fluids released from the crystallizing mafic body in which the abundance of magmatic amphibole revealed the high water content of this mafic magma. Finally, the whole complex is intruded by a new pulse at 442 ± 5 Ma crosscutting magmatic flow structures associated to the diorite intrusion.

8.2. Cotectic and non-cotectic trends

A debated topic about calc-alkaline granite rocks concerns the possibility that granitoids represent either liquids fractionated from a parental intermediate magma of broadly diorite composition or, by contrast, they represent magmas formed by partial melting of crustal sources. In the latter possibility, the high content Fe and Mg of the magmas ("maficity") can be explained by the inclusion of suspended mafic material (entrained restites) from the source (e.g., Clemens et al., 2011); with the consequent reduction of magma temperature (T < 900 °C) if maficity is not an essential part of the liquid. By contrast, if maficity is considered to be an intrinsic feature of the silicate liquid, the implication is that high temperatures (>1000 °C) are required to make these Fe- and Mg-rich liquids stable at crustal pressures. Consequently, whether rock compositions represent liquid systems or not, is a central part of the discussion about the origin, crustal or not, of calc-alkaline granite batholiths.

If magmas are produced by fractionation from a parental mafic magma, they will follow cotectic patterns in major-element geochemical variation diagrams. By contrast, trends produced by variable entrainment of restitic material from the source or any other type of mechanical separation of liquid and crystals will produce rectilinear, non-cotectic, trends as those reported from "cumulative granites" of the Lachlan fold belt in Australia (Chappell and Wyborn, 2004), formed by incomplete separation of restite and melt, and those reported from the Stepninsk pluton in the Urals (Bea et al., 2005). Other cases of non-cotectic geochemical variation have been reported as resulting from bulk assimilation of country rocks (Díaz-Alvarado et al., 2011).

Comparison with experimental melts from systems of intermediate composition (andesitic or dioritic) reveals that most samples of the Palanche pluton are arranged along geochemical trends that can be compared with cotectic liquids. We refer these patterns as cotectic lines of liquids (CLL; Castro, 2013) and not as *liquid lines of descent* (LLD) as early defined by Bowen (1928). The difference is that liquids aligned along a cotectic pattern represent liquid batches, whose compositions are in equilibrium with a saturating solid assemblage at different temperatures (cotectic). They may differ from liquids that are derived by fractional crystallization from a magma. We prefer to use the term cotectic lines of liquid to refer to equilibrium compositions and not fractionated liquids.

Most samples of the Palanche tonalite–granite series fall on the cotectic lines of the F–An–Or pseudoternary projection (Fig. 13). Mafic enclaves plot in the area of andesites and close to the parental andesite system used in experiments with cotectic liquids referred above (blue star in Fig. 13b). These enclaves and dismembered mafic bodies may represent the parental magmas of the Palanche cotectic trends. Inset in Fig. 13b represents hypothetical phase equilibria, as based on experimental assemblages and melt compositions. These fairly reproduce the mineralogy and textures of Palanche granitoids with peritectic reactions from Px to Hbl and Hbl to Bt. Note that several samples of the Palanche series with compositions ranging from MgO = 1.0 to 1.5 wt.%, together with samples of the Cueva del Chacho granodiorite, depart from the cotectic line, pointing to the field of country rocks, in this case represented by greywackes of the Puncoviscana Neoproterozoic sediments. Enrichment in MgO and K_2O, coupled with increasing alumina saturation index (parameter A in Fig. 13d), are proofs of local contamination with pelitic country rocks. For comparative purposes, the S/I transitional granites of the SVB (Grosse et al., 2011) are plotted in the diagrams, showing that they result of bulk assimilation of pelitic material (yellow star in Fig. 13) by magmas similar to the calc-alkaline cotectic trend of Palanche. Samples richer in K_2O and poorer in CaO (CaO < 1.0 wt.%, molar K# > 0.8) of the transitional series may represent either assimilation by the more evolved terms of the cotectic series or incomplete unmixing between anatectic melts and restitic minerals from the pelitic source (Fig. 13a, c). The rest of the transitional samples are clearly contaminated.

9. Conclusions

The southern tip of SVB is excellent scenery to study the build-up of batholiths in general and the Sierra de Velasco in particular. Most samples of the Palanche pluton are arranged along geochemical trends that can be compared with cotectic liquids, traced from experimental liquid compositions of calc-alkaline (andesitic) systems. Mafic enclaves and dismembered bodies, present in abundance in the granitoids, may represent the parental magma of the Palanche cotectic trends: an intermediate system of andesite composition (SiO_2 > 55 wt.%) with initial water content of about 2.5 wt.% H_2O as maximum.

Local assimilation of country rocks produced non-cotectic trends characterized by enrichment in MgO and K_2O, coupled with increasing alumina saturation index.

The field and age relations of the tonalite–monzogranite series of the Palanche pluton indicate that uniform processes of melting and fractionation were operative for at least 40 Ma. Several pulses of magma were in-situ fractionated at about472 Ma, and intruded later by mafic rocks (456 Ma), under magmatic conditions in the host granitoids. The magmatism continued until at least 442 Ma, when a new pulse intruded into the oldest rocks.

Acknowledgments

Most data contained in this paper are part of the PhD Thesis of the first author (LIB). The Consejo Nacional de Investigaciones Científicas y Técnicas (CONICET) is thanked for scholarships awarded to L. Bellos during her PhD studies. She would like to thank CIUNT for the financial support through projects 26/G321–26/G439. Additional sampling in 2009, petrology and SHRIMP studies were funded with research grants from the Spanish Research Commission (PLUVOLC project CGL2010-22022-C02-01) and the Andalusian Government (Proyecto de Excelencia

P09-RNM-5378). Part of the radiometric determinations was performed in the SHRIMP-IBERSIMS laboratory (Granada) and part in the Beijing SHRIMP Center (P.R. China). This paper is the publication Nº 13 of the IBERSIMS Lab, which is leaded by Fernando Bea and Pilar Montero. We thank Xie Hangqiang for assistance with SHRIMP work in Beijing and Juana Rossi and José Pablo López for their comments.

Appendix A. Supplementary data

Supplementary data to this article can be found online at http://dx.doi.org/10.1016/j.gr.2013.09.019.

References

Aceñolaza, F.G., Toselli, A.J., 1981. Geología del Noroeste Argentino. Publicación especial, 1287. Facultad de Ciencias Naturales, UNT, Tucumán, Argentina (212 pp.).
Aceñolaza, F.G., Miller, H., Toselli, A.J., 1996. Geología del Sistema de Famatina. Münchner Geologische Hefte, Reihe A19, 412.
Annen, C., Scaillet, B., Sparks, R.S.J., 2006. Thermal constraints on the emplacement rate of a large intrusive complex: the Manaslu leucogranite, Nepal Himalaya. Journal of Petrology 47, 71–95.
Báez, M.A., Basei, M.A., 2005. El plutón San Blas, magmatismo posdeformacional Carbonífero en la Sierra de Velasco. Serie de Correlación Geológica 19, 239–246.
Báez, M.A., Bellos, L.I., Grosse, P., Sardi, F.G., 2005. Caracterización petrológica de la Sierra de Velasco. In: Dahlquist, J.A., Rapela, C.W., Baldo, E. (Eds.), Geología de la provincia de La Rioja –Precámbrico-Paleozoico Inferior. Asociación Geológica Argentina, Serie D, publicación especial, 8, pp. 123–130.
Baldo, E.G., Murra, J.A., Casquet, C., Galindo, C., Saavedra, J., 1999. El gabro coronítico de la Sierra de Valle Fértil, Sierras Pampeanas, Argentina: condiciones P-T de la etapa coronítica. Boletín de la Sociedad Española de Mineralogía 22-A, 17–18.
Barbarin, B., 2005. Mafic magmatic enclaves and mafic rocks associated with some granitoids of the central Sierra Nevada batholith, California: nature, origin, and relations with the hosts. Lithos 80, 155–177.
Bea, F., 2010. Crystallization dynamics of granite magma chambers in the absence of regional stress: multiphysics modeling with natural examples. Journal of Petrology 51, 1541–1569.
Bea, F., 2012. The sources of energy for crustal melting and the geochemistry of heat-producing elements. Lithos 153, 278–291.
Bea, F., Montero, P., Zinger, T., 2003. The nature, origin, and thermal influence of the granite source layer of Central Iberia. Journal of Petrology 111, 579–595.
Bea, F., Fershtater, G.B., Montero, P., Smirnov, V.N., Molina, J.F., 2005. Deformation-driven differentiation of granitic magma: the Stepninsk pluton of the Uralides, Russia. Lithos 81, 209–233.
Bellos, L., 2005. Geología y petrología del sector austral de la sierra de Velasco, al sur de los 29º 44′S, La Rioja, Argentina. In: Aceñolaza, F.G., Hünicken, M., Toselli, A.J., Aceñolaza, G.F. (Eds.), Serie de Correlación Geológica, 19, pp. 261–278.
Bellos, L.I., Toselli, A.J., Rossi, J.N., Grosse, P., de la Rosa, J.D., Castro, A., 2010. Caracterización petrográfica y geoquímica y condiciones de deformación del plutón San Cristóbal, Sierra de Velasco (La Rioja, Argentina). Estudios Geológicos 66, 157–169.
Bowen, N.L., 1928. The Evolution of the Igneous Rocks. Dover Publications, New York (332 pp.).
Castro, A., 2013. Tonalite–granodiorite suites as cotectic systems: a review of experimental studies with applications to granitoid petrogenesis. Earth Science Reviews 124, 68–95.
Castro, A., Moreno-Ventas, I., De la Rosa, J., 1990. Microgranular enclaves as indicators of hybridization processes in granitoid rocks, Hercynian belt, Spain. Geological Journal 25, 391–404.
Castro, A., Moreno-Ventas, I., Fernández, C., Vujovich, G., Gallastegui, G., Heredia, N., Martino, R.D., Becchio, R., Corretgé, L.G., Díaz-Alvarado, J., Such, P., García-Arias, M., Liu, D.Y., 2011. Petrology and SHRIMP U–Pb zircon geochronology of Cordilleran granitoids of the Bariloche area, Argentina. Journal of South American Earth Sciences 32, 508–530.
Castro, A., Díaz-Alvarado, J., Fernández, C., 2014. Fractionation and incipient self-granulitization during deep-crust emplacement of Lower Ordovician Valle Fértil batholith at the Gondwana active margin of South America. Gondwana Research 25, 685–706.
Castro, A., Vogt, K., Gerya, T.V., 2013. Generation of new continental crust by sublithospheric silicic-magma relamination in arcs: a test of Taylor's andesite model. Gondwana Research 23, 1554–1566.
Chappell, B.W., White, A.J.R., 1974. Two contrasting granite types. Pacific Geology 8, 173–174.
Chappell, B.W., Wyborn, D., 2004. Cumulate and cumulative granites and associated rocks. Resource Geology 54, 227–240.
Cisterna, C.E., 2001. Volcanismo subácueo en el Eopaleozoico del Sistema de Famatina, noroeste de Argentina. Revista de la Asociación Geológica Argentina 56, 16–24.
Clemens, J.D., Stevens, G., Farina, F., 2011. The enigmatic sources of I-type granites: the peritectic connexion. Lithos 126, 174–181.
Coira, B., Pérez, B., Flores, P., Kay, S.M., Woll, B., Hanning, M., 1999. Magmatic sources and tectonic setting of Gondwana margin Ordovician magmas, northern Puna of Argentina and Chile. In: Ramos, V., Keppie, J. (Eds.), Laurentia–Gondwana connections before Pangea. Geological Society of America, Special Papers, 336, pp. 145–170.
Coleman, D.S., Gray, W., Glazner, A.F., 2004. Rethinking the emplacement and evolution of zoned plutons: geochronologic evidence for incremental assembly of the Tuolumne Intrusive Suite, California. Geology 32, 433–436.
Dahlquist, J.A., Rapela, C.W., Pankhurst, R.J., Baldo, E.G., Saavedra, J., y Alasino, P.H., 2005. Los granitoides de la Sierra de Chepes y su comparación con granitoides paleozoicos de las Sierras Pampeanas: implicancias para el orógeno Famatiniano. In: Dahlquist, J.A., Rapela, C.W., Baldo, E. (Eds.), Geología de la provincia de La Rioja –Precámbrico-Paleozoico Inferior. Asociación Geológica Argentina, Serie D, publicación especial, 8, pp. 87–108.
Dahlquist, J.A., Pankhurst, R.J., Rapela, C.W., Casquet, C., Fanning, C.M., Alasino, P., Báez, M.A., 2006. The San Blas pluton: an example of Carboniferous plutonism in the Sierras Pampeanas, Argentina. Journal of South American Earth Sciences 20, 341–350.
Dahlquist, J.A., Alasino, P.H., Eby, N., Galindo, C., Casquet, C., 2010. Fault controlled Carboniferous A-type magmatism in the proto-Andean foreland (Sierras Pampeanas, Argentina): geochemical constraints and petrogenesis. Lithos 115, 65–81.
De los Hoyos, C.R., Willner, A.P., Larrovere, M.A., Rossi, J.N., Basei, M.A.S., 2011. Tectonothermal evolution and exhumation history of the Paleozoic Proto-Andean Gondwana margin crust: the Famatinian Belt in NW Argentina. Gondwana Research 20, 309–324.
De los Hoyos, C.R., Willner, A.P., Larrovere, M.A., Rossi, J.N., Toselli, A.J., 2009. Thermobarometry and geochronology of metapelites and granitoids of the eastern Sierra de Velasco, Sierras Pampeanas, Argentina: P–T paths and exhumation rates during the Famatinian Cycle. Proceedings XXI Latin American Colloquium. Göttingen, Germany pp. 77–79.
Debon, F., Le Fort, P., 1983. A chemical–mineralogical classification of common plutonic rocks and association. Transaction of the Royal Society of Edinburgh: Earth Sciences 73, 135–149.
Díaz-Alvarado, J., Castro, A., Fernandez, C., Moreno-Ventas, I., 2011. Assessing bulk assimilation in cordierite-bearing granitoids from the central system batholith, Spain; experimental, geochemical and geochronological constraints. Journal of Petrology 52, 223–256.
Díaz-Alvarado, J., Castro, A., Fernández, C., Moreno-Ventas, I., 2013. SHRIMP U–Pb zircon geochronology and thermal modeling of multilayer granitoid intrusions. Implications for the building and thermal evolution of the Central System batholith, Iberian Massif, Spain. Lithos 175–176, 104–123.
Drobe, M., López de Luchi, M., Steenken, A., Frei, R., Naumann, R., Siegesmund, S., Wemmer, K., 2009. Provenance of the late Proterozoic to early Cambrian metaclastic sediments of the Sierra de San Luis (eastern Sierras Pampeanas) and Cordillera Oriental, Argentina. Journal of South American Earth Sciences 28, 239–262.
Durand, F.R., López, J.P., 1996. La deformación dúctil en el flanco oriental del Sistema de Famatina. In: Aceñolaza, F., Miller, H., Toselli, A.J. (Eds.), Geología de Sistema de Famatina. Münchner Geologische Hefte, Rehihe A, 19, pp. 311–323.
Finney, S.C., Gleason, J.D., Gehrels, G.E., Peralta, S., Aceñolaza, G., 2003. Early Gondwanan connection for the Argentine Precordillera terrane. Earth and Planetary Science Letters 205, 349–359.
Frost, B.R., Barnes, C.G., Collins, W.J., Arculus, R.J., Ellis, D.J., Frost, C.D., 2001. A geochemical classification for granitic rocks. Journal of Petrology 42, 2033–2048.
Glazner, A.F., Bartley, J.M., Coleman, D.S., Gray, W., Taylor, R.Z., 2004. Are plutons assembled over millions of years by amalgamation from small magma chambers. GSA Today 14, 4–11.
González Bonorino, F., 1950. Algunos problemas geológicos de las Sierras Pampeanas. Revista de la Asociación Geológica Argentina 5, 81–110.
González Bonorino, F., 1951. Una nueva Formación Precámbrica en el Noroeste Argentino. Comunicaciones Científicas del Museo de La Plata 5, 4–6.
Grosse, P., Sardi, F.G., 2005. Geología de los granitos Huaco y Sanagasta, sector centro-oriental de la Sierra de Velasco, La Rioja. In: Aceñolaza, F.G., Aceñolaza, G., Hünicken, M., Rossi, J.N., Toselli, A.J. (Eds.), Serie Correlación Geológica, 19, pp. 221–238.
Grosse, P., Söllner, F., Báez, M.A., Toselli, A.J., Rossi, J.N., de la Rosa, J.D., 2009. Lower Carboniferous post-orogenic granites in central-eastern Sierra de Velasco, Sierras Pampeanas, Argentina: U–Pb monazite geochronology, geochemistry and Sr–Nd isotopes. International Journal of Earth Sciences 98, 1001–1025.
Grosse, P., Bellos, L.I., de los Hoyos, C.R., Larrovere, M.A., Rossi, J.N., Toselli, A.J., 2011. Across-arc variation of the Famatinian magmatic arc (NW Argentina) exemplified by I-, S and transitional I/S-type Early Ordovician granitoids of the Sierra de Velasco. Journal of South American Earth Sciences 32, 110–126.
Hervé, F., Pankhurst, R.J., Fanning, C.M., Calderon, M., Yaxley, G.M., 2007. The South Patagonian batholith: 150 my of granite magmatism on a plate margin. Lithos 97, 373–394.
Hibbard, M.J., 1991. Textural anatomy of twelve magma-mixed granitoid systems. In: Didier, J., Barbarin, B. (Eds.), Enclaves and Granite Petrology. Developments in Petrology, 13, pp. 431–444.
Höckenreiner, M., Söllner, F., Miller, H., 2003. Dating the TIPA shear zone: an Early Devonian terrane boundary between Famatinian and Pampean system (NW-Argentina). Journal of South American Earth Sciences 16, 45–66.
Isacks, B., 1988. Uplift of the central Andean plateau and bending of the Bolivian Orocline. Journal of Geophysical Research B93, 3211–3231.
Jordan, T.E., Allmendinger, R.W., 1986. The Sierras Pampeanas of Argentina: a modern analogue of Rocky Mountain foreland deformation. American Journal of Science 286, 737–764.
Kelemen, P.B., Hanghoj, K., Greene, A.R., 2003. One view of the geochemistry of subduction-related magmatic arcs, with emphasis on primitive andesite and lower crust. In: Rudnick, R.L. (Ed.), The Crust. Elsevier, Amsterdam, pp. 593–659.
Kretz, R., 1983. Symbols for rock-forming minerals. American Mineralogist 68, 277–279.
Leake, B.E., Woolley, A.R., Arps, C.E.S., Birch, W.D., Gilbert, M.C., Grice, J.D., Hawthorne, F.C., Kato, A., Kisch, H.J., Krivovichev, V.G., Linthout, K., Laird, J., Mandarino, J.A., Maresch, W.V., Nickel, E.H., Rock, N.M.S., Schumacher, J.C., Smith, D.C., Stephenson, N.C.N., Ungaretti, L., Whittaker, E.J.W., Youshi, G., 1997. Nomenclature of amphiboles: report of the subcommittee on amphiboles of the International Mineralogical Association,

Commission on New Minerals and Mineral Names. American Mineralogist 82, 1019–1037.
Lee, C.-T.A., Morton, D.M., Kistler, R.W., Baird, A.K., 2007. Petrology and tectonics of Phanerozoic continent formation: from island arcs to accretion and continental arc magmatism. Earth and Planetary Science Letters 263, 370–387.
López, J.P., Bellos, L.I., Grosse, P., 2006. Estructura y petrografía de zonas de cizalla en la sierra de Velasco, La Rioja. Asociación Geológica Argentina, Serie D, publicación especial, 9 201–206.
Lucassen, F., Franz, G., 2005. The early Paleozoic Orogen in the Central Andes: a non-collisional orogen compatible to the Cenozoic high plateau? In: Vaughan, A.P.M., Leat, P.T., Pankhurst, R.J. (Eds.), Terrane Processes at the Margins of Gondwana. Geological Society, Special Publications, 246, pp. 257–273.
Maaloe, S., Wyllie, P.J., 1975. Water content of a granite magma deduced from the sequence of crystallization determined experimentally with water-undersaturated conditions. Contributions to Mineralogy and Petrology 52, 175–191.
Mannhein, R., Miller, H., 1996. Las rocas volcánicas y subvolcánicas eopaleozoicas del sistema de Famatina. In: Aceñolaza, F.G., Miller, H., Toselli, A.J. (Eds.), Geología del Sistema de Famatina. Münchner Geologische (Hefte A), 19, pp. 159–186.
Martino, R.D., Guereschi, A.B., Sfragula, J.A., 2009. Petrology, structure and tectonic significance of the Tuclame banded schists in the Sierras Pampeanas of Córdoba and its relationship with the metamorphic basement of northwestern Argentina. Journal of South American Earth Sciences 27, 280–298.
Miller, C.F., Furbish, D.J., Walker, B.A., Claiborne, L.L., Koteas, G.C., Bleick, H.A., Miller, J.S., 2011. Growth of plutons by incremental emplacement of sheets in crystal rich host: evidence from Miocene intrusions of the Colorado River region, Nevada, USA. Tectonophysics 500, 65–77.
Miller, H., Söllner, F., 2005. The Famatina complex (NW-Argentina): back-docking of an island arc or terrane accretion? Early Palaeozoic geodynamics at the western Gondwana margin. In: Vaughan, A.P.M., Leat, P.T., Pankhurst, R.J. (Eds.), Terrane Processes at the Margins of Gondwana. Geological Society of London, Special Publications, 246, pp. 241–256.
Murra, J., Baldo, E., 2006. El metamorfismo de las rocas básicas y ultrabásicas de la Sierra de la Huerta- Las Imanas (Sierras Pampeanas, Argentina): caracterización tectonotérmica del margen occidental del orógeno Famatiniano. Revista Geologica de Chile 33, 277–298.
Naney, M.T., 1983. Phase equilibria of rock forming ferromagnesian silicates in granitic systems. American Journal of Science 283, 993–1033.
Otamendi, J.E., Ducea, M.N., Tibaldi, A.M., Bergantz, G.W., de la Rosa, J.D., Vujovich, G.I., 2009a. Generation of tonalitic and dioritic magmas by coupled partial melting of gabbroic and metasedimentary rocks within the deep crust of the Famatinian magmatic arc, Argentina. Journal of Petrology 50, 841–873.
Otamendi, J.E., Vujovich, G.I., de la Rosa, J.D., Tibaldi, A.M., Castro, A., Martino, R.D., Pinotti, L.P., 2009b. Geology and petrology of a deep crustal zone from the famatinian paleo-arc: Sierras de Valle Fértil y La Huerta, San Juan, Argentina. Journal of South American Earth Sciences 27, 258–279.
Otamendi, J.E., Ducea, M.N., Bergantz, G.W., 2012. Geological, petrological and geochemical evidence for progressive construction of an arc crustal section, Sierra de Valle Fértil, Famatinian Arc, Argentina. Journal of Petrology 53, 761–800.
Pankhurst, R.J., Rapela, C.W., 1998. The proto-Andean margin of Gondwana: an introduction. In: Pankhurst, R.J., Rapela, C.W. (Eds.), The Proto-Andean Margin of Gondwana. Geological Society of London, Special Publications, 142, pp. 1–10.
Pankhurst, R., Rapela, C., Saavedra, J., Baldo, E., Dahlquist, J., Pascua, I., Fanning, C.M., 1998. The Famatinian magmatic arc in the central Sierras Pampeanas: an Early to Mid-Ordovician continental arc on the Gondwana margin. In: Pankhurst, R., Rapela, C. (Eds.), The Proto-Andes Margin of Gondwana. Geological Society, London, Special Publications, 142, pp. 343–367.
Pankhurst, R.J., Weaver, S.D., Hervé, F., Larrondo, P., 1999. Mesozoic–cenozoic evolution of the North Patagonian batholith in Aysén, Southern Chile. Journal of the Geological Society (London) 156, 673–694.
Pankhurst, R., Rapela, C., Fanning, C., 2000. Age and origin of coeval TTG, I- and S- type granites in the Famatinian belt of NW Argentina. Transactions of the Royal Society of Edinburgh: Earth Sciences 91, 151–168.
Paterson, S.R., Vernon, R.H., 1995. Bursting the bubble of ballooning plutons: a return to nested diapirs emplaced by multiple processes. Geological Society of America Bulletin 107, 1356–1380.
Paterson, S.R., Okaya, D., Memeti, V., Economos, R., Miller, R.B., 2011. Magma addition and flux calculations of incrementally constructed magma chambers in continental margin arcs: combined field, geochronologic, and thermal modeling studies. Geosphere 7, 1439–1468.
Pearce, J.A., Harris, N.B.W., Tindle, A.G., 1984. Trace element discrimination diagrams for the tectonic interpretation of granites rocks. Journal of Petrology 25, 956–983.
Pichavant, M., Macdonald, R., 2007. Crystallization of primitive basaltic magmas at crustal pressures and genesis of the calc-alkaline igneous suite: experimental evidence from St Vincent, Lesser Antilles arc. Contributions to Mineralogy and Petrology 154, 535–558.
Pichavant, M., Kontak, D.J., Briqueu, L., Herrera, J.V., Clark, A.H., 1988a. The Miocene–Pliocene Macusani volcanics, SE Peru — II. Geochemistry and origin of a felsic peraluminous magma. Contributions to Mineralogy and Petrology 100, 325–338.
Pichavant, M., Kontak, D.J., Herrera, J.V., Clark, A.H., 1988b. The Miocene–Pliocene Macusani volcanics, SE Peru — I. Mineralogy and magmatic evolution of a two-mica aluminosilicate-bearing ignimbrite suite. Contributions to Mineralogy and Petrology 100, 300–324.
Presnall, D.C., Bateman, P.C., 1973. Fusion relations in the system $NaAlSi_3O_8$–$CaAl_2Si_2O_8$–$KAlSi_3O_8$–SiO_2–H_2O and generation of granitic magmas in the Sierra Nevada batholith. Geological Society of America Bulletin 84, 3181–3201.
Rapela, C.W., Coira, B., Toselli, A., Saavedra, J., 1992. The lower Paleozoic magmatism of southwestern Gondwana and the evolution of Famatinian orogene. International Geology Review 34, 1081–1142.
Rapela, C.W., Pankhurst, R.J., Casquet, C., Fanning, C.M., Baldo, E.G., González-Casado, J.M., Galindo, C., Dahlquist, J.A., 2007. The Río de La Plata craton and the assembly of SW Gondwana. Earth-Science Reviews 83, 49–82.
Rossi, J.N., Toselli, A.J., Saavedra, J., Sial, A.N., Pellitero, E., Ferreira, V.P., 2002. Common crustal source for contrasting peraluminous facies in the Early Paleozoic Capillitas batholith, NW Argentina. Gondwana Research 5, 325–337.
Saal, A., Toselli, A.J., Rossi de Toselli, J.N., 1996. Granitoides y rocas básicas de la Sierra de Paganzo. In: Aceñolaza, F.G., Miller, H., Toselli, A.J. (Eds.), Geología del Sistema de Famatina. Münchner Geologische Hefte, Rehihe, A19, pp. 199–209.
Saavedra, J., Toselli, A.J., Rossi, J.N., Pellitero, E., Durand, F., 1998. The Early Paleozoic magmatic record of the Famatina system: a review. In: Pankhurst, R.J., Rapela, C.W. (Eds.), The Proto-Andean Margin of Gondwana. Geological Society of London, Special Publications, 142, pp. 283–295.
Sun, S.S., McDonough, W.F., 1989. Chemical and isotopic systematic of oceanic basalts: implications for mantle composition and processes. In: Saunders, A.D., Norry, M.J. (Eds.), Magmatism in ocean basins. Geological Society of London, Special Publication, 42, pp. 313–345.
Tepper, J.H., Kuehner, S.M., 2004. Geochemistry of mafic enclaves and host granitoids from the Chilliwack batholith, Washington: chemical exchange processes between coexisting mafic and felsic magmas and implications for the interpretation of enclave chemical traits. Journal of Geology 112, 349–367.
Tobisch, O.T., McNulty, B.A., Vernon, R.H., 1997. Microgranitoid enclave swarms in granitic plutons, central Sierra Nevada, California. Lithos 40, 321–339.
Toselli, A.J., Saavedra, J., Pellitero, E., Rossi de toselli, J.N., Aceñolaza, F.G., Medina, M.E., 1990. Geoquímica y petrogénesis del volcanismo Ordovícico de la Formación las Planchadas, Sistema de Famatina. Revista de la Asociación Geológica Argentina 45, 313–322.
Toselli, A.J., Miller, H., Saavedra, J., Rossi de Toselli, J.N., Pellitero, E., 1996. Granitoides y rocas básicas de la Sierra de Paimán. In: Aceñolaza, F., Miller, H., Toselli, A. (Eds.), Geología del Sistema de Famatina. Münchner Geologische Hefte, Rehihe, A19, pp. 241–253.
Toselli, A.J., Rossi, J.N., Sardi, F., López, J., Báez, M., 2000. Caracterización petrográfica y geoquímica de granitoides de la sierra de Velasco, La Rioja, Argentina. 17 Geowissenschaftliches latinamerika – kolloquium (17 LAK). Profil, 18:38 (6 pp.).
Toselli, A.J., Rossi, J.N., Miller, H., Báez, M.A., Grosse, P., López, J.P., Bellos, L.I., 2005. Las rocas graníticas y metamórficas de la Sierra de Velasco. In: Aceñolaza, F.G., Aceñolaza, G., Hünicken, M., Rossi, J.N., Toselli, A.J. (Eds.), Serie Correlación Geológica, 19, pp. 211–220.
Toselli, A.J., Miller, H., Aceñolaza, F.G., Rossi, J.N., Söllner, F., 2007. The Sierra de Velasco (northwestern Argentina) — an example for polyphase magmatism at the margin of Gondwana. Neues Jahrbuch für Geologie und Paläontologie 246, 325–345.
Vernon, R.H., Etheridge, M.A., Wall, V.J., 1988. Shape and microstructure of microgranitoid enclaves. Indicators of magma mingling and flow. Lithos 22, 1–11.
Viramonte, J.M., Becchio, R.A., Viramonte, J.G., Pimentel, M.M., Martino, R.D., 2007. Ordovician igneous and metamorphic units in southeastern Puna: new U–Pb and Sm–Nd data and implications for the evolution of northwestern Argentina. Journal of South American Earth Sciences 24, 167–183.
Zorpi, M.J., Coulon, C., Orsini, J.B., Cocirta, C., 1989. Magma mingling, zoning and emplacement in calc-alkaline granitoid plutons. Tectonophysics 157, 315–329.